National Library
of Canada

Acquisitions and
Bibliographic Services Branch

395 Wellington Street
Ottawa, Ontario
K1A 0N4

Bibliothèque nationale
du Canada

Direction des acquisitions et
des services bibliographiques

395, rue Wellington
Ottawa (Ontario)
K1A 0N4

Your file Votre référence

Our file Notre référence

NOTICE

The quality of this microform is heavily dependent upon the quality of the original thesis submitted for microfilming. Every effort has been made to ensure the highest quality of reproduction possible.

If pages are missing, contact the university which granted the degree.

Some pages may have indistinct print especially if the original pages were typed with a poor typewriter ribbon or if the university sent us an inferior photocopy.

Reproduction in full or in part of this microform is governed by the Canadian Copyright Act, R.S.C. 1970, c. C-30, and subsequent amendments.

AVIS

La qualité de cette microforme dépend grandement de la qualité de la thèse soumise au microfilmage. Nous avons tout fait pour assurer une qualité supérieure de reproduction.

S'il manque des pages, veuillez communiquer avec l'université qui a conféré le grade.

La qualité d'impression de certaines pages peut laisser à désirer, surtout si les pages originales ont été dactylographiées à l'aide d'un ruban usé ou si l'université nous a fait parvenir une photocopie de qualité inférieure.

La reproduction, même partielle, de cette microforme est soumise à la Loi canadienne sur le droit d'auteur, SRC 1970, c. C-30, et ses amendements subséquents.

Canada

UNIVERSITY OF ALBERTA

POLYMER WAVEGUIDES WITH TAPS IN SILICON V-GROOVES

BY

SENTHIL BALASUBRAMANIAN KUMAR

©

A thesis submitted to the faculty of Graduate Studies and Research in partial fulfillment of the requirements for the degree of Master of Science.

DEPARTMENT OF ELECTRICAL ENGINEERING

Edmonton, Alberta

Fall 1992

National Library of Canada
Bibliothèque nationale du Canada

Canadian Theses Service
Service des thèses canadiennes

Ottawa, Canada
K1A 0N4

The author has granted an irrevocable non-exclusive licence allowing the National Library of Canada to reproduce, loan, distribute or sell copies of his/her thesis by any means and in any form or format, making this thesis available to interested persons.

L'auteur a accordé une licence irrévocable et non exclusive permettant à la Bibliothèque nationale du Canada de reproduire, prêter, distribuer ou vendre des copies de sa thèse de quelque manière et sous quelque forme que ce soit pour mettre des exemplaires de cette thèse à la disposition des personnes intéressées.

The author retains ownership of the copyright in his/her thesis. Neither the thesis nor substantial extracts from it may be printed or otherwise reproduced without his/her permission.

L'auteur conserve la propriété du droit d'auteur qui protège sa thèse. Ni la thèse ni des extraits substantiels de celle-ci ne doivent être imprimés ou autrement reproduits sans son autorisation.

ISBN 0-315-77082-1

Canada

UNIVERSITY OF ALBERTA

RELEASE FORM

NAME OF AUTHOR: SENTHIL BALASUBRAMANIAN KUMAR

TITLE OF THESIS: POLYMER WAVEGUIDES WITH TAPS IN SILICON V-GROOVES

DEGREE: MASTER OF SCIENCE

YEAR THIS DEGREE GRANTED: 1992

Permission is hereby granted to the University of Alberta Library to reproduce single copies of this thesis and to lend or sell such copies for private, scholarly or scientific purposes only.

The author reserves all other publication and other rights in association with the copyright in the thesis, and except as hereinbefore provided neither the thesis nor any substantial portion thereof may be printed or otherwise reproduced in any material form whatever without the author's prior written permission.

36, TVS Nagar
Edayarpalayam post
Coimbatore, Tamil Nadu
India 641025

Date: October 8, 1992

UNIVERSITY OF ALBERTA

FACULTY OF GRADUATE STUDIES AND RESEARCH

The undersigned certify that they have read, and recommend to the Faculty of Graduate Studies and Research for acceptance, a thesis entitled POLYMER WAVEGUIDES WITH TAPS IN SILICON V-GROOVES submitted by SENTHIL BALASUBRAMANIAN KUMAR in partial fulfillment of the requirements for the degree of MASTER OF SCIENCE.

Dr. J. N. McMullin, Supervisor

Dr. R. I. MacDonald, Supervisor

Dr. B. Keyworth

Dr. W. Finlay

Date: 24 Sept '92

ABSTRACT

Polymer optical waveguides with low loss have been developed in silicon v-grooves. Integrated sidewall taps and end facets which tap light out-of-plane have been fabricated by silicon micromachining. The design, fabrication and testing of a 12 x 12 tapping array is given along with a demonstration of fiber to waveguide coupling using alignment grooves.

Acknowledgments

I would like to express my sincere gratitude to my supervisors Dr. J. N. McMullin and Dr. R. I. MacDonald, for their support and guidance throughout this project. I have benefited greatly from their advice and encouragement.

I would like to thank Graham Mckinnon for arranging for the necessary resources at the Alberta Microelectronic Centre to complete this project. I also thank him for the help and advice given at the various stages of this project.

I would also like to take this opportunity to thank the following people for their assistance:

Glen Fitzpatrick, for the chemical vapour depositions of oxide, assistance in the development of a process for the metallization of taps and for the SEM pictures.

Yan Loke, for training me in photolithography and silicon micromachining and for the constant help and encouragement.

Alan Mitchell, for electron beam evaporation of aluminum and spectrophotometer runs.

Harold Peacock, for assistance during mask design.

Dr. M. C. Williams of the Chemical Eng. Dept., for his advice on polymers.

Rajashree Narendra, for the help and useful discussions.

TABLE OF CONTENTS

	PAGE
CHAPTER 1 INTRODUCTION	1
1.1 Optical Interconnects	1
1.2 Choice of Substrate	1
1.3 Waveguide Structures on Silicon	3
1.4 Application of Imbedded Channel Waveguide	5
1.5 Outline of Thesis	7
CHAPTER 2 FABRICATION OF POLYMER OPTICAL WAVEGUIDES	9
2.1 Introduction	9
2.2 Requirements of the Core Material	10
2.3 Waveguide Fabrication	12
2.3.1 Photolithography	13
2.3.2 Crystal planes and anisotropic etching	15
2.3.3 Deposition of the buffer layer	16
2.3.4 Metallization of coupling planes	18
2.3.5 Application of core material	19
2.3.6 Application of cladding	23
2.3.7 End polishing for butt-coupling	23
CHAPTER 3 EVALUATION OF WAVEGUIDE LOSSES	25
3.1 Introduction	25
3.2 Experimental Setup for Measuring Intrinsic Polymer Losses	27
3.3 Experimental Setup for Measuring Waveguide Losses	29
3.4 Loss Results for Polymer Waveguides	31
3.4.1 Losses in waveguides made by grinding and polishing	31
3.4.2 Losses in waveguides made by doctorblading	35

PAGE

CHAPTER 4 WAVEGUIDE TAPS AND FIBER SELF-ALIGNMENT 39

4.1 Introduction 39

4.2 Undercutting Phenomenon at Corners 39

4.3 Types of Taps 41

4.4 Etching Profiles of Rectangular Masks 43

4.5 Calculation of Attenuation in a Waveguide with Three Inside Taps and One End Facet 46

4.6 Design of Inside Taps 47

4.7 A 12 x 12 Tapping Array for a Hybrid Optoelectronic Switch Matrix 50

4.7.1 Design of tapping array and alignment grooves 50

4.7.2 Fabrication of the array 51

4.7.3 Testing of a waveguide with 12 taps 51

4.8 Demonstration of Fiber to Waveguide Coupling using Alignment Grooves 53

4.8.1 Fabrication process 56

4.8.2 Assembly of fiber in alignment groove 57

4.8.3 Loss measurements 57

CHAPTER 5 CONCLUSION 60

5.1 Summary of Work 60

5.2 Feasibility in Commercial Applications 60

5.3 Suggestions for Future Work 61

BIBLIOGRAPHY 63

APPENDIX A SUMMARY OF EVALUATION OF OPTICAL MATERIALS 66

APPENDIX B PROPERTIES OF MATERIALS 67

APPENDIX C POSITIVE PHOTORESIST PHOTOLITHOGRAPHY RECIPE 69

PAGE

APPENDIX D MASKS USED FOR DEVELOPING WAVEGUIDES AND TAPS 70

APPENDIX E METALLIZATION OF TAPS 75

APPENDIX F ALIGNMENT OF FIBER PROBE TO WAVEGUIDE 78

APPENDIX G DERIVATION OF TAPPING SIZE D_n 80

APPENDIX H DETERMINATION OF ETCH RATE OF (212)-(212) CORNER 81

APPENDIX I DESIGN OF TAPPING ARRAY WITH ALIGNMENT GROOVES 82

LIST OF FIGURES

		PAGE
Fig. 1.1 (a)	Cross-section of planar waveguide	4
Fig. 1.1 (b)	Cross-section of ridge channel waveguide	4
Fig. 1.1 (c)	Cross-section of imbedded channel waveguide	4
Fig. 1.2 (a)	Schematic of waveguide with optical taps	6
Fig. 1.2 (b)	A 4 x 4 integrated optoelectronic switch matrix	6
Fig. 2.1	Cross-section of ideal multimode waveguide	9
Fig. 2.2	Wafer processing steps for v-groove formation	14
Fig. 2.3	Hydrated SiO_2 residue at bottom of groove near a tap	17
Fig. 2.4	Nodules of oxide formed on Al during CVD	17
Fig. 2.5	Formation of polymer waveguide	21
Fig. 2.6 (a)	Cross-sectional view of waveguide with doctorbladed core	22
Fig. 2.6 (b)	Top surface of waveguide with doctorbladed core	22
Fig. 2.7	Cross-sectional view of complete waveguide	24
Fig. 3.1	Setup for measuring intrinsic polymer losses	28
Fig. 3.2	Scattered power from polymer in between microscope slides	28
Fig. 3.3	Setup for measuring losses in waveguides	30
Fig. 3.4	Scattered power from waveguide with no buffer layer	32
Fig. 3.5	Scattered power from waveguide with 0.6 μm SiO_2 buffer layer	32
Fig. 3.6	Scattered power from waveguide with 1 μm SiO_2 buffer layer	33
Fig. 3.7	Scattered power from waveguide with 2 μm SiO_2 buffer layer	33
Fig. 3.8	Scattered power from waveguide with 3 μm SiO_2 buffer layer	34
Fig. 3.9	Scattered power from waveguide with 2 μm SiO_2 buffer layer and upper cladding layer	34

		PAGE
Fig. 3.10	Scattered power from waveguide with 2.6 μm SiO_2 buffer layer (doctorbladed core material)	36
Fig. 3.11	Scattered power from waveguide with 3 μm SiO_2 buffer layer (doctorbladed core material)	36
Fig. 3.12	Scattered power from waveguide with Al on 3 μm SiO_2 buffer layer (doctorbladed core material)	38
Fig. 4.1	Facets at an undercut corner	40
Fig. 4.2 (a)	Etch window for waveguide with three outside taps	42
Fig. 4.2 (b)	V-groove with etched outside tap and end facet	42
Fig. 4.3 (a)	Etch window for waveguide with three inside taps	42
Fig. 4.3 (b)	V-groove with etched inside tap and end facet	42
Fig. 4.4	View of inside tap from end of waveguide groove	43
Fig. 4.5 (a)	Successive etching shapes with a rectangular mask	44
Fig. 4.5 (b)	Etched shape at point a	44
Fig. 4.5 (c)	Etched shape at point b	44
Fig. 4.5 (c)	Etched shape at point P	44
Fig. 4.6 (a)	Photograph of inside tap with etching stopped at point P	45
Fig. 4.6 (b)	Photograph of inside tap with etching continued beyond P	45
Fig. 4.7	Scattered power from waveguide with three inside taps and one end facet	46
Fig. 4.8	Cross-sectional view of waveguide with tap	48
Fig. 4.9	Construction of rectangular mask for given D_n	48
Fig. 4.10	SEM photograph of the tapping array after EPW etching	52
Fig. 4.11	Results of tap measurements	52
Fig. 4.12	Pictures of taps showing the presence of an interface plane	54
Fig. 4.13 (a)	Schematic of alignment groove and waveguide	55

PAGE

Fig. 4.13 (b) Fiber assembled in alignment groove after making a saw cut to remove the intermediate silicon 55

Fig. 4.14 Photographs of single fiber assembled in alignment groove 58

LIST OF ACRONYMS AND ABBREVIATIONS

AMC	Alberta Microelectronic Centre
BOE	Buffered Oxide Etch
CCD	Charge Coupled Device
COR	Centre of Rotation
CVD	Chemical Vapour Deposition
DI	Deionised
dia.	diameter
EPW	Ethylenediamine-Pyrocatechol-Water
JFET	Junction Field-Effect Transistor
LED	Light Emitting Diode
MM	Multimode
NA	Numerical Aperture
NOA	Norland Optical Adhesive
OEIC	Optoelectronic Integrated Circuit
PCB	Printed Circuit Board
rpm	revolutions per minute
sccm	standard cubic centimetre per minute
SEM	Scanning Electron Microscope
SLS	Strained Layer Superlattices
TRLabs	Telecommunications Research Laboratories
UV	Ultraviolet
VLSI	Very Large Scale Integration

CHAPTER 1

INTRODUCTION

1.1 Optical Interconnects

Optical interconnects have been proposed to overcome the shortcomings of electrical interconnects in the development of high speed systems (>1 GHz) as they offer larger bandwidths, low crosstalk, larger fanouts and lend themselves to multiplexing and switching [1-4], which automatically leads to a reduction in the number of physical interconnections, decrease in power consumption and higher packing densities in integrated circuits. Optical interconnects are also used as signal distribution media in integrated optics. An optical interconnect generally consists of a source, typically a laser diode or LED, an optical channel and a receiver consisting of a detector and an amplifier. Optical channels which are being used nowadays include optical fibers, integrated optical waveguides and, under laboratory development, free space propagation using lenses and holograms [2,4]. For inter-chip connections, **integrated optical waveguides** are attractive because lasers and detectors can be integrated onto the waveguides in a monolithic or hybrid fashion and they occupy less volume [4] than the other optical channels mentioned above.

1.2 Choice of Substrate

There are many substrates on which optical waveguides can be realized such as semiconductors (Si, III/V compounds) and dielectrics ($LiNbO_3$). The choice of substrate would depend on the function which has to be implemented. $LiNbO_3$ is a commonly used material in integrated optics because it exhibits the piezoelectric and electro-optic effects.

Titanium diffused into $LiNbO_3$ is often used to create a waveguide and waveguide losses of the order of 0.5 dB/cm have been achieved [5]. With the exception of emitters and detectors, most other integrated optics components have been demonstrated with $LiNbO_3$ [6].

Semiconductors would be a natural choice if one has to integrate electronics with optics. Active devices like lasers and detectors can be fabricated on direct energy gap semiconductors like GaAs and related compounds. GaAs is also preferred for its speed and resistance to radiation. On the other hand, Si has a well-developed materials and processing technology and has the following desirable properties in its use as a substrate material :

a) Si allows for the formation of silicon dioxide on its surface which is chemically stable and acts as a protective layer and has good waveguiding properties.
b) It has a high thermal conductivity and this is utilized in heat dissipation in lasers and amplifiers.
c) Si wafers can align optical components with great stability since the thermal expansion coefficient of Si is close to that of glass. Coupling losses of less than 0.03 dB over a 100°C temperature range for fiber to waveguide coupling have been obtained [7].
d) Si can be micromachined to hold fibers, lenses, etc. by utilizing the various crystal plane orientations that can be preferentially etched to form desired microstructures. Since lithographic precision of the order of 0.5 microns can be obtained, excellent alignment precisions can achieved [7].

Active optoelectronic devices in Si would allow for integration of the device with the substrate and eliminate losses that would normally occur if the device were butt-coupled to the waveguide. However, there is a difficulty in making optical emitters from silicon because of its indirect energy gap. Si also does not exhibit the electro-optic effect. Progress has been made in recent years to eliminate these deficiencies. Despite the lattice

mismatch of about 4% between Si and III-V compounds, GaAs/AlGaAs lasers have recently been grown on silicon and have exhibited pulsed operation and low threshold [8]. Photodetectors can be made by laser recrystallisation of Si. An integrated photodetector array has been demonstrated in laser recrystallised silicon deposited on a Si_3N_4 optical waveguide with the individual photodiodes having low reverse current ($<10^{-9}$A) and break down voltage of 24V [9]. Electro-optic effects have also been observed in laser-annealed ZnO on silicon [9] and in Ge-Si strained-layer superlattices (SLS) [8].

1.3 Waveguide Structures on Silicon

There are three general geometries of optical waveguides which can be realized on Si : planar , ridge channel and imbedded channel waveguides as shown in Fig. 1.1 . In all these types of waveguides, a buffer layer (usually SiO_2) of adequate thickness is deposited or grown on the silicon substrate to prevent coupling of light into the absorbing substrate. The core material which has a refractive index larger than the buffer layer is then deposited followed by an optional upper cladding which has a lower refractive index than the core material. For planar waveguides, core materials such as Si_3N_4, Ta_2O_5, Nb_2O_5, ZnO, 7059 glass, undoped and phosphorous-doped SiO_2, organic materials and barium silicate have been tried [10]. The lowest losses that have ever been obtained on silicon substrate were obtained with deposited ZnO and Corning 7059 glass which were subsequently laser-annealed to reduce the scattering loss introduced by the fabrication process. Laser-annealed ZnO showed a loss of 0.01 dB/cm while 7059 glass showed a loss of 0.05 dB/cm which was reduced to 0.01 dB/cm by applying a surface coating [9].

The ridge and imbedded channel waveguides provide additional lateral confinement to that provided by the planar waveguide. The ridge channel waveguide is formed by planar growth or deposition followed by lateral structuring by chemical etching or physical erosion. Low losses are obtained if the walls of the waveguide are smooth. Losses of 1 - 2 dB/cm at 514.5 nm have been obtained in phosphosilicate glass (PSG)

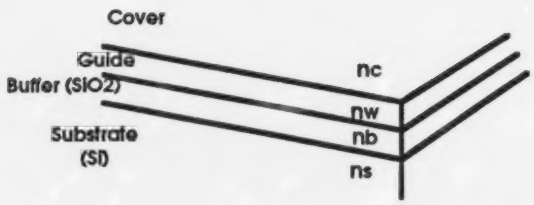

$n_c < n_w < n_b$

(a) Cross-section of planar waveguide

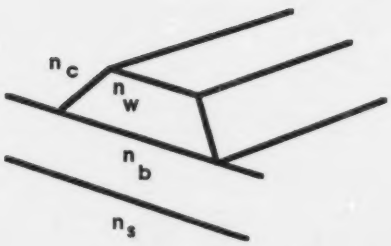

(b) Cross-section of ridge channel waveguide

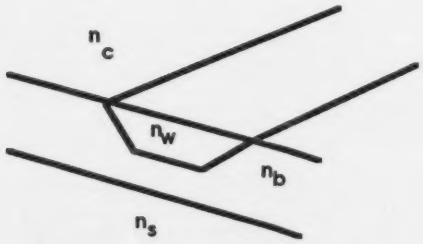

(c) Cross-section of imbedded channel waveguide

Fig. 1.1

which has undergone reflow by heat treatment to smoothen any sharp edges that may have occurred in the fabrication process [9].

Imbedded channel waveguides may be formed by preferential etching of certain crystal planes followed by deposition or growth of a SiO_2 layer and then a deposition of a core material. The sidewalls formed are extremely smooth and contribute to the low loss. Larger channels can be etched in line with the waveguide channels for placing optical fibers for light coupling. Epoxy [11], plastic [12, 13] and sputtered glass [14] have been tried as the waveguiding material. Losses obtained have been in the 2 - 4 dB/cm range. Devices using imbedded channel waveguides such as an optical beam splitter [14] has been demonstrated and a CCD multiplexer [15] has been proposed. Three-dimensional integrated optics using out-of-plane coupling from silicon v-grooves has also been described [13].

1.4 Application of Imbedded Channel Waveguide

In this thesis, we describe the development of channel waveguides with around 1 dB/cm propagating loss using polymers in preferentially etched silicon and demonstrate their application in a waveguide with serial out-of-plane taps. A schematic of a waveguide with serial out-of-plane taps is shown in Fig. 1.2 (a). It is basically a power splitter whose function is to divide and direct the incoming light energy into n photodetectors denoted by circles mounted on the surface of the substrate (n being 4 in this example). Such a tapped waveguide could be used for distributing clock signals on boards or within chips in VLSI circuits. Another application of tapped waveguides could be in a hybrid integrated version of the optoelectronic switch matrix which has been developed at TRLabs [16]. The advantage of using a hybrid integrated version of an optoelectronic switch matrix is the simplified optical power splitting and the larger number of cross points per unit area permissible for the same performance. A 4x4 switch would consist of 4 waveguides each having 4 out-of-plane taps placed side by side as shown in Fig. 1.2 (b).

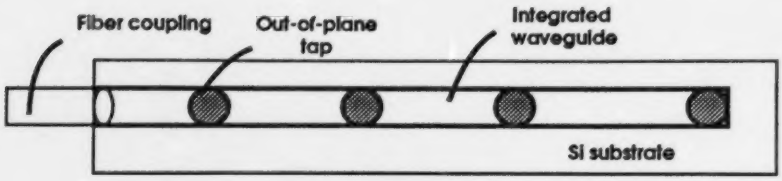

(a) Schematic of waveguide with optical taps

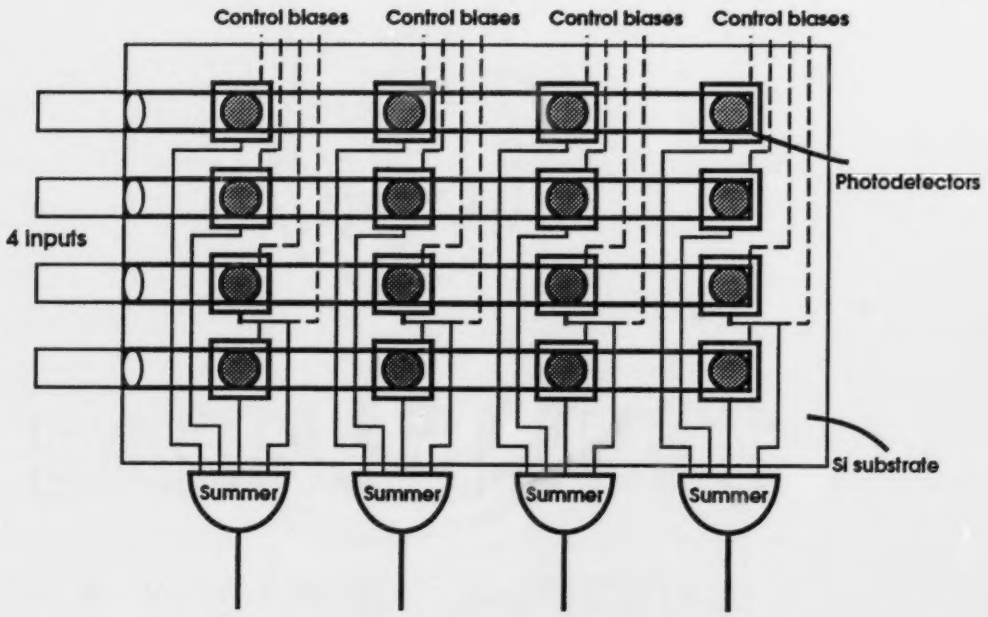

(b) A 4x4 integrated optoelectronic switch matrix

Fig. 1.2

The input to each waveguide is information-modulated light. The information is available at all tap points on the waveguide. Photodetectors are integrated in a hybrid fashion over each tap. All the photodetectors across each column in the 4x4 matrix are connected in parallel and the outputs given to 4 summers. If information is to be routed from one of the inputs to a particular output, the corresponding photodetector at the crosspoint is turned on by biasing it with an appropriate voltage [17].

The modulated laser energy is coupled to the waveguide with multimode optical fibers. Since the waveguide uses a v-groove geometry, the fiber could be coupled and aligned on the v-groove with high precision and low coupling loss [15]. The waveguides are multimode and have dimensions of the order of 100 μm which reduce coupling difficulties usually associated with single mode waveguides. Since the distances involved are a few centimetres, the modal dispersion is negligible [18]. The photodetectors, either photoconductors or photodiodes, could be epoxied on to the taps and electrical connections could be made with metallized interconnections on the silicon. The signal available at each summing point is amplified before further processing (such as electrical to optical conversion) to usable signal levels. Important figures of merit of an optoelectronic switch are the crosstalk between channels, the reconfiguration time of the switch (detector on/off time) and the detection bandwidth of the crosspoint. Optoelectronic switches have applications in communications switching, delay line processors, look-up tables for residue arithmetic, optoelectronic neural networks and mixer arrays [16].

1.5 Outline of Thesis

Chapter 2 describes the fabrication of polymer waveguides. The steps required for deposition of aluminum selectively on taps in the waveguide are also described in this chapter. Chapter 3 presents the loss results obtained in the waveguides along with the experimental setup. In Chapter 4, we introduce the phenomenon of corner undercutting and describe how two types of sidewall taps can be micromachined in the v-grooves. The

fabrication and testing of a 12 x 12 tapping array is given along with a demonstration of fiber to waveguide coupling using alignment grooves. Chapter 5 summarizes the achievements made and recommends areas for future work.

CHAPTER 2

FABRICATION OF POLYMER OPTICAL WAVEGUIDES

2.1 Introduction

The structure of the waveguide we would ideally like to realize is a multimode waveguide with a triangular core (Fig. 2.1). The layer on top of the silicon surface is a buffer layer of silicon dioxide which isolates the core of the waveguide from the high index and absorbing silicon substrate. It should be of sufficient thickness so that the evanescent fields of the propagating modes do not extend to the lossy substrate. The core of the waveguide should have a refractive index larger than the buffer layer, so that light is confined by total internal reflection. This layer is typically tens of microns thick for multimode waveguides. A lower refractive index cladding is deposited at the top surface of

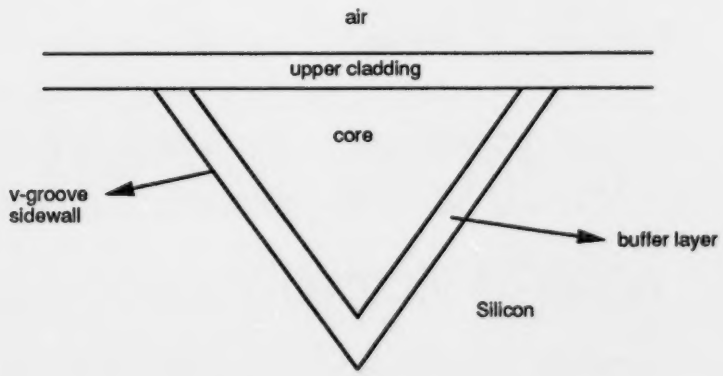

Fig. 2.1 Cross-section of ideal multimode waveguide (diagram not to scale)

the core so as to reduce scattering losses by decreasing the effective surface perturbation seen by the propagating mode. In the following sections, the selection of the core material and the fabrication of a complete waveguide will be discussed.

2.2 Requirements of the Core Material

Since the waveguide is to be used in a hybrid optoelectronic circuit, the materials used in the waveguide should meet certain requirements. They are listed below :

(1) Low propagation loss

The loss acceptable in the waveguide would depend on the power budget. If we assume an optical path length of 50 mm between the various elements and that we would like to keep the propagation losses under 5 dB, then the requirement would be less than 1 dB/cm loss. This means that the material used as the core should possess (a) a high transmission in the wavelengths of interest (600 to 1550 nm) and (b) uniformity in refractive index so that scattering losses are reduced. The waveguide should be fabricated such that losses due to surface roughness are minimal.

(2) Refractive index

The refractive index of the core should be higher than the index of SiO_2. Also it would be advantageous if variations of the material are available with a lower refractive index to act as a cladding layer.

(3) Film quality

It should be possible to deposit thick layers (>100 μm) without cracks and material shrinkage. The deposition method must be such that the thickness is repeatable. There should be no bubbles as they will increase the scattering losses.

(4) Environmental stability [19]

The material should retain its optical properties under varying environmental conditions. Factors like adhesion, stress resistance, wide temperature tolerances and

imperviousness to humidity are important properties of environmentally stable materials. Adhesion of the material to SiO_2 was a problem with many of the materials we tested.

(5) Hardness

Initially, the procedure we followed for making the waveguide was to deposit a thick layer of the material over the buffer layer and then grind and polish down the material down to the v-groove surface using successively finer abrasives. It was important at that time to have a hard material which would not warp during grinding and polishing with the silicon carbide and alumina abrasives (hardness 9 and 8 on the Mohs' scale respectively). With our final procedure of spreading the material on the surface with a sharp edge rubber blade, henceforth referred to as "doctorblading", we have made the polishing step a simpler one by actually not abrading the material. Hardness, therefore is not an important factor if the material can be doctorbladed into the v-groove.

Based on these requirements, we looked at different methods and materials for waveguide deposition and evaluated their performance. The chemical vapour deposition system at the AMC was not able to deposit more than 20 μm of doped oxide without the oxide cracking due to stress build-up [20], and was hence ruled out. We focused on solution-deposited films as a means of getting thicker films. Organic materials were a natural choice since many transparent polymers such as epoxies, resins and acrylics exist which have refractive indices in the range 1.5 to 1.7 [21]. Organic and polymeric materials are frequently used in integrated optics since they have a number of desirable properties such as fabrication flexibility, low absorption in the spectral range of interest, minimal scattering defects, and the tailoring of optical properties via molecular engineering [22]. Also a number of organic materials have been developed recently which are optically active and exhibit effects such as the electro-optic effect and electro-refraction [23]. We looked at commercially available polymers as potential waveguiding materials. Their performance was evaluated by depositing the material on the buffer layer, curing it and grinding and

polishing down the material to the v-groove surface. A summary of the results of the materials evaluated is given in Appendix A.

The most suitable material we encountered was an optical adhesive from Norland Products Inc. It comes in the form of a clear , colourless, solvent-free liquid which is cured by ultra-violet light (350 nm). The material is said to have excellent adhesion to glass and low shrinkage. Since it is a one-component material, the possibility of bubble formation usually associated with two-component materials is much reduced. Since the material does not have a solvent to outgas, it is possible to form thick layers without cracking during curing. Variations of the product exist with refractive indices in the range 1.524 to 1.56 at λ =587 nm. The three Norland adhesives used were NOA 61, NOA 81 and NOA 68. Their properties are given in Appendix B. These Norland adhesives have been used as ridge channel waveguides formed by laser direct writing [24] and selective polymerization [25]. Losses obtained were in the range of 0.4 to 0.6 dB/cm suggesting that they are very low loss materials. In Sections 2.3.5 and 2.3.6, the method of use of these polymers will be explained.

2.3 Waveguide Fabrication

The steps required for the making of the waveguide are:

a) Photolithography

b) Anisotropic etching for v-groove formation

c) Deposition of buffer layer of SiO_2

d) Metallization of coupling planes

e) Application of core material

f) Application of cladding

g) End polishing for butt coupling

2.3.1 Photolithography

This is the process wherein the geometric pattern which has to be etched into a v-groove is transferred to the surface of the wafer. The process is depicted in Fig. 2.2. The full recipe of the photolithographic process is given in Appendix C. A four inch (100)-oriented Si wafer (usually p-doped) was thermally oxidized in a nitrogen-water vapour atmosphere in a quartz furnace for one hour. A thin layer (~0.5 μm) of silicon dioxide grew on both surfaces of the wafer. This acts as a mask for all the subsequent wafer processing steps.

Next a thin uniform layer (~1.4 μm thick) of positive photoresist (HPR 504) was deposited on the wafer by spinning. The wafer was then softbaked in a preheated oven. This process removes the excess solvent present in the photoresist and dries the film.

The next step is the selective exposure of the photoresist to ultraviolet light using a contact printer. The mask containing the waveguide patterns was clamped on the mask aligner. Pictures of the masks used in this work are shown in Appendix D. The wafer was placed on a vacuum chuck and made to come very close to the mask. The primary flat of the Si wafer was aligned to one of the alignment marks on the mask. This process is critical for proper orientation of the v-groove sidewalls. After alignment was done, the wafer was made to contact the mask and the mask was exposed for 11 seconds to a 200 watt mercury lamp which emits ~5mJ/cm^2. The wafer was taken and developed in the spinner. The developer used was Shipley 354. The resist dissolved in areas where it was exposed and the unexposed regions remained intact as shown in step 3 of Fig. 2.2. The wafer was inspected under a microscope to verify that the image has been accurately transferred.

The wafer was hardbaked prior to etching to improve the adhesion of the photoresist to the oxide. The photoresist is etch-resistant to 10:1 buffered oxide etch (BOE; 10 parts by vol. Ammonium fluoride (40%) and 1 part by vol. hydrofluoric acid (49%)) The wafer was coated on the back surface with a plastic adhesive to protect the oxide from being etched. The wafers were dipped in the BOE for 10 to 15 minutes and then put in a

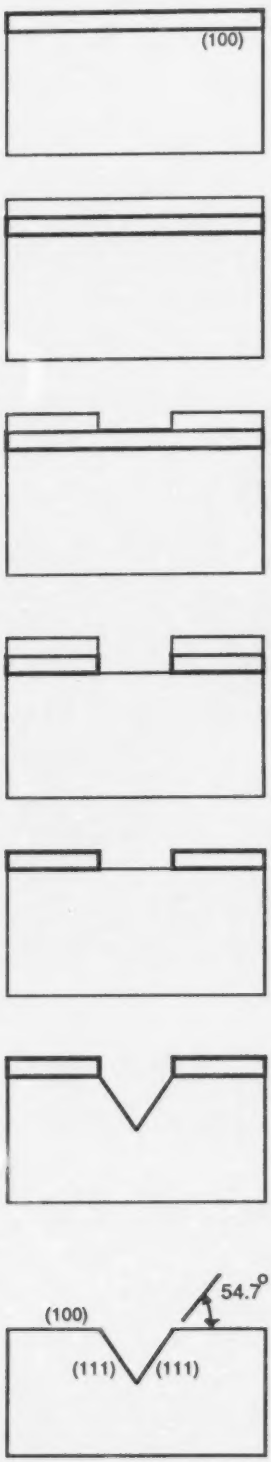

(100) oriented silicon wafer with thermally oxidized $Si0_2$

Spin photoresist and soft bake

Align mask, expose, develop and hard bake

Remove exposed oxide using buffered oxide etch

Strip photoresist using acetone

Anisotropic etching using ethylenediamine-pyrocatechol-water

Remove oxide using buffered oxide etch

Fig. 2.2 Wafer processing steps for v-groove formation

water cascade for 1/2 hour to remove impurities. The areas of oxide not covered with photoresist were etched away exposing the Si surface as shown in step 4. The next step is to strip the photoresist. This was done by washing the wafer in acetone. The wafer was cleaned with deionised water and dried with pure nitrogen gas. The wafer was then ready for anisotropic etching.

2.3.2 Crystal planes and anisotropic etching

The crystal structure of silicon is a diamond type face centered cubic lattice. Any crystal plane in the silicon crystal lattice can be identified by a set of numbers called Miller indices which are obtained by determining the intercepts of the plane on a three coordinate axis [26]. To determine the Miller indices, the origin of the coordinate system is first made to coincide with a lattice site in one of these planes. If the next parallel plane in that set has intercepts on the x-, y-, and z-axes at x_1, y_1 and z_1, then the reciprocal of these numbers each multiplied by a common integer gives three integers and the three smallest integers are referred to as the Miller indices h, k and l. They are written in parenthesis as (h k l). If any of the intercepts, for example the x intercept, is negative then it is denoted by with a bar on the corresponding Miller index such as ($\bar{h}$ k l). The crystallographic direction is denoted by angular brackets such as <h k l> and its direction is normal to the (h k l) plane. The angle ø between two crystallographic directions denoted by <h_1 k_1 l_1> and <h_2 k_2 l_2> is given by

$$\text{ø} = \cos\text{-}1\left[\frac{h_1h_2 + k_1k_2 + l_1l_2}{(h_1^2 + k_1^2 + l_1^2)^{1/2}(h_2^2 + k_2^2 + l_2^2)^{1/2}}\right]$$

Of the many planes possible in the crystal structure, the (100), (111) and (110) planes are the most important. Certain etchants have the property that the etch rate varies with direction. One such etchant is a mixture of ethylenediamine, pyrocatechol and water (EPW) at 115°C. The mixing ratio is 750 ml ethylenediamine, 120 gm pyrocatechol and 240 ml of deionised water. This EPW mixture etches in the <100> direction about 35 times

faster than the <111> direction. The reason for this is the high atomic packing density of the <111> direction as compared to the <100> direction. It etches SiO_2 at a very slow rate (2 A°/min) and hence SiO_2 is used as a mask. The resulting etching of any opening in the mask of a (100) wafer is to produce smooth (111) sidewalls which are oriented at 54.74° to the (100) surface. If the etching is allowed to proceed, the sidewalls eventually meet to form a v-groove as shown in step 7 of Fig. 2.2. The wafers with patterned oxide were placed in a glass holder and immersed in the preheated EPW solution. The solution was homogenized by a magnetic stirrer activated by an external rotor. If the samples were not immediately processed after patterning, a BOE dip for 15 seconds is required to remove any oxide unintentionally grown on the exposed silicon. The wafers are etched for 2 - 2.5 hours depending on the depth of the groove to be etched. The observed etch rate was ~0.64 μm/min. The etch rate was found to increase with the age of the EPW solution. A one-day-old solution etches as fast as 1.3 μm/min. After etching, the wafers were cleaned in a water cascade and blown dry. The v-grooves were examined under a microscope to verify quality. We observed occasionally the presence of a white residue in the grooves which prevented the etching of the underlying Si by EPW [Fig. 2.3]. This polymeric form of hydrated SiO_2 [27] occurs in EPW solutions which are used for more than a day. To avoid this problem, it was necessary to make fresh solutions of EPW every time.

2.3.3 Deposition of the buffer layer [20]

The buffer layer of oxide was deposited using chemical vapour deposition. In this method, silane (SiH_4) reacts with oxygen at 440°C and 300 mTorr. The reaction is:

$$SiH_4 + O_2 \xrightarrow{440^\circ C} SiO_2 + H_2O$$

The flow rates of silane and oxygen are 84 sccm and 144 sccm respectively. The deposition rate was ~120 A°/min. The thickness of oxide at the edges of a 4-inch diameter wafer was a 10 to 15 % less than in the centre of the wafer. Since the thickness of the buffer layer necessary to prevent absorption of the mode in the Si substrate was not exactly

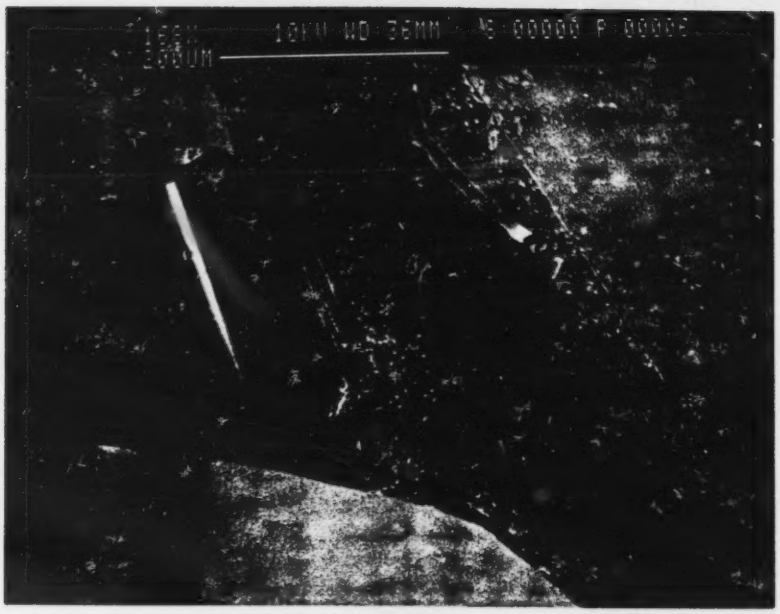

Fig. 2.3 Hydrated SiO_2 residue at bottom of groove near a tap

Fig. 2.4 Nodules of oxide formed on Al during CVD

known, we had to deposit various thicknesses and measure the attenuation in the waveguide. The wafers were rinsed with DI water and dried prior to the CVD process.

2.3.4 Metallization of coupling planes

When taps are fabricated at the same time as the v-groove is fabricated as described in Chapter 4, it is necessary to increase the coupling efficiency of these taps by coating them with highly reflective material such as aluminum (Al) or silver (Ag) as silicon has poor reflectivity (~ 35% at 630 nm, air-Si at normal incidence). Ideally, we would like the reflective layer beneath the oxide all over the wafer since it would be a simple process. However, nodule formation of CVD SiO_2 on sputtered Al was observed. These nodules occurred in various sizes (1μm to 10 μm in dia.) and resulted in a rough SiO_2 surface as shown in Fig. 2.4. This phenomenon has been attributed [28] to the recrystallisation of Al due to the elevated temperature of the CVD operation which results in nuclei formation and subsequent nucleated growth of SiO_2. Use of this buffer layer in a waveguide would result in large number of scattering centres because the size of these nodules is comparable to the wavelength of light. We also found that other methods of Al deposition such as thermal evaporation and electron beam evaporation produced nodules with differing densities. Other highly reflective films with high melting points (960°C) such as silver resulted in major degradation in reflectivity. Hence we decided to deposit the reflective layer on top of the buffer layer and only at the taps since our own measurements have shown that a loss of about 2.4 dB/cm would be obtained in a waveguide (doctorbladed type) with 0.1 μm Al on top of 3 μm SiO_2. The high loss observed is due to the finite conductivity of Al.

The process for metallizing the taps uses negative resist patterning and was developed at the AMC. In this process, spots of photoresist were made on the wafer coated with a buffer layer and Al. An Al etch solution removes the Al in all places except under these photoresist spots. The resist was washed away using a xylene solution leaving the

reflective Al spots in the desired places. The detailed sequence of steps for defining Al selectively on the taps is given in appendix E.

2.3.5 Application of core material

The core materials tried were NOA 61 and NOA 81. Two methods of applying the core material evolved. In the first method, the adhesive was dispensed using the squeezable container on v-grooves on the wafer where the adhesive was desired. A microscope glass slide was used to spread the adhesive more uniformly on the wafer. To remove any bubbles which may be present in the liquid, the sample was kept in a vacuum jar (pressure -80 KPa) for at least 5 minutes. The sample was next cured to a hard film under a 200 watt mercury lamp emitting ~5mJ/cm^2 for 10 minutes (NOA 81) and 20 minutes (NOA 61). The thick layer of polymer was then reduced to a reasonably smooth surface by a process of grinding and polishing. The apparatus used was a grinder/polisher with an 8" wheel with controllable rotation rate between 50 to 500 rpm. Abrasive papers or polishing cloths were clamped onto the wheel. When an abrasive disc was on the wheel, water from a spout lubricated the grinding process and flushed away the abraded material. For the polishing cloths, a slurry of the powder and DI water was used. The procedure followed was:

Abrasive grit size	particle size(μm)	wheel rpm	criteria for time
400 grit	22	200	Should remove 90% of excess thickness
600 grit soft	14	200	Should remove 400 grit scratches
800 grit	9.5	200	Should remove 600 grit scratches
Levigated Al2O3	5	150	Should remove 800 grit scratches
Micropolish II deaglomerrated a alumina	1	150	Should remove 5 μm powder scratches
Micropolish II deaglomerrated g alumina	0.05	150	Should remove 1 μm powder scratches

The polishing times varied from 15 to 30 minutes for small wafer pieces (about 0.5"x 1.0") to about 3 hours for whole 4" dia. wafers. The polymer had a depression of ~3

μm in the centre of the groove due to the abrasive action of the polishing powders on the soft polymer. The surface has irregular scratch patterns of < 1 μm rms roughness. The sides of the waveguides were also pitted due to seepage of abrasive powders into the v-groove sidewalls. Increasing the buffer layer thickness beyond 2 μm did not bring down the loss of 3.2 dB/cm. It became necessary to develop a new method of fabrication.

Fig. 2.5 depicts the steps required to form the polymer waveguide using the second method. The adhesive is dispensed at the required places in the same way as before. Bubbles are removed using a vacuum jar. Next, a rubber sheet with a sharp edge is used to doctorblade the adhesive with adequate pressure along the length of the waveguide to remove the excess. If too much pressure is applied, the rubber at the edge gets depressed into the v-groove forcing the liquid out resulting in a very large depression. The doctorblading is repeated until the adhesive retracts into the v-groove all along the length of the waveguide. This process results in the formation of a concave surface of the adhesive in the v-groove which is extremely smooth due to the surface tension of the liquid. The adhesive has a maximum depression of about 20 μm for a 128 μm wide waveguide. The adhesive is cured as before and the excess polymer outside the v-groove is easily removed using a 600 grit soft abrasive paper. The concave nature of the polymer surface prevents the abrasion of the core and this is critical in obtaining low loss. Surface roughening is encountered at the edge of the waveguide due to abrasive action on the polymer and this contributes to wide fluctuations in the scattered power (See Section 3.4.2). Though the exact loss is hard to determine because of these fluctuations, the losses are lower than are obtained in waveguides made by grinding and polishing the polymer. Using a smaller grit (800) for removing excess polymer aggravates the roughness problem as it takes longer to remove the excess polymer. Fig. 2.6 (a) and (b) shows a picture of the cross-section and top surface of the doctorbladed and polished waveguide respectively.

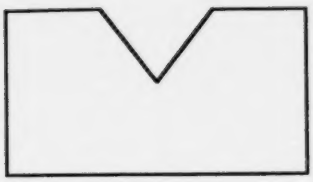

Etch a v-groove in (100) oriented silicon wafer

Deposit a buffer layer of SiO_2 using chemical vapour deposition (CVD) and pattern Al reflective spots

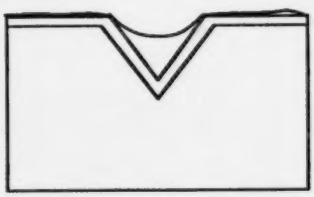

Coat with polymer, doctor blade and cure

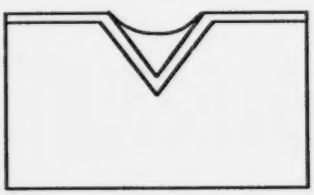

Remove excess polymer with 600 grit soft abrasive paper

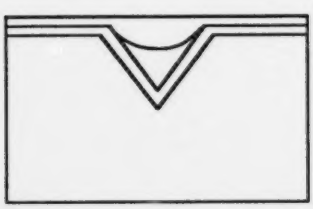

Spin on cladding layer and polish ends for coupling

Fig. 2.5 Formation of polymer waveguide

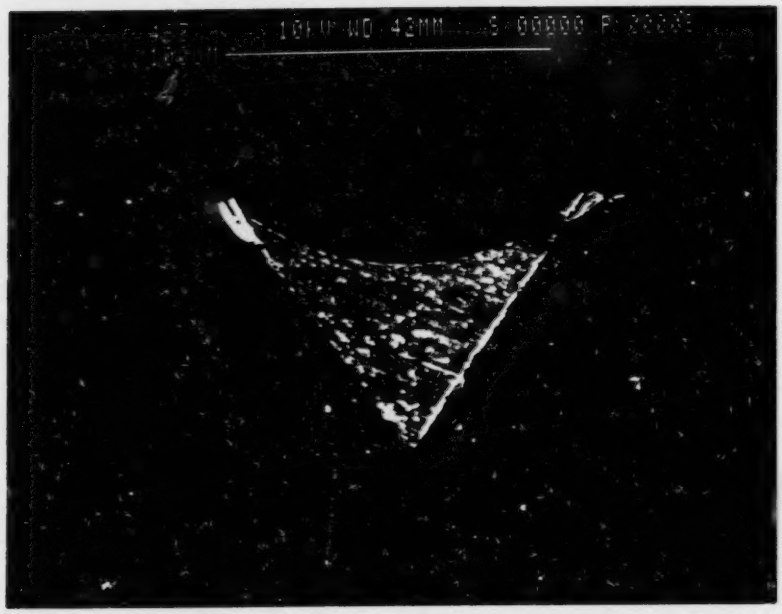

Fig. 2.6 (a) Cross-sectional view of waveguide with doctorbladed core

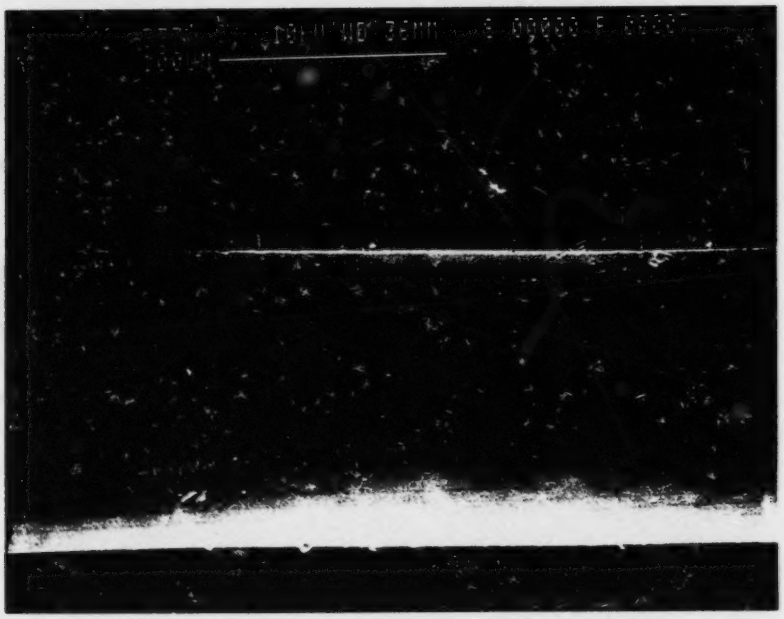

Fig. 2.6 (b) Top surface of waveguide with doctorbladed core

2.3.6 Application of cladding

A smooth-surfaced cladding layer was formed by spinning on NOA 68 ($n_c = 1.54$) on the core of the waveguide. The cladding layer reduces the scattering losses and the upper numerical aperture is reduced to 0.25. The cladding also offers mechanical protection to the core.

The sample is placed on the vacuum chuck of the spinner and the adhesive was dispensed from its container. Due to its high viscosity, it was necessary to spread the adhesive manually all over the sample using a glass microscope slide. The spin speed depends on the desired thickness of the cladding; the larger the spin speed, the smaller the thickness produced. For a spin-on time of 15 seconds, a maximum thickness of 55 μm was obtained at a spin speed of 5000 rpm. The adhesive was then cured for 10 minutes under the UV lamp.

2.3.7 End polishing for butt-coupling

Since the light beam is to be coupled to the waveguide via a multimode fiber, it is necessary to prepare the input end of the waveguide to smoothness to reduce coupling losses. This is achieved by grinding away the silicon with a 400 grit abrasive disc until the end of the waveguide is flush with the edge of the sample. This was followed by polishing with a 1 μm mean roughness glass plate and the ends are observed under a microscope for flatness and smoothness. A SEM picture of the cross-section of the complete waveguide is shown in Fig. 2.7.

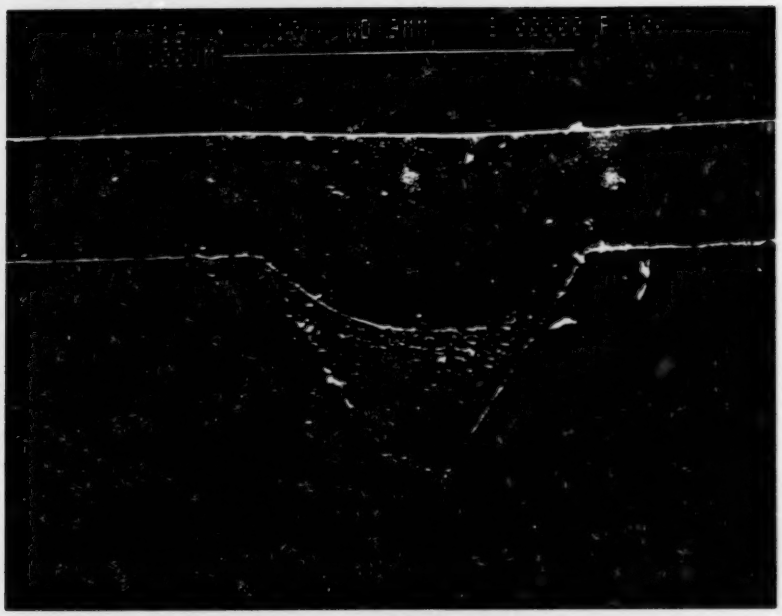

Fig. 2.7 Cross-sectional view of complete waveguide

CHAPTER 3

EVALUATION OF WAVEGUIDE LOSSES

3.1 Introduction

There are many mechanisms by which power losses could occur in optical waveguides. For straight waveguides, the losses include [5]:

a) Absorption losses

These are due to impurity absorption, interband absorption etc. in the waveguiding materials. These losses are important in semiconductor waveguides.

b) Scattering losses

These losses are due to the imperfections in the waveguides such as surface roughness and inconsistency in refractive index in the waveguiding material. In effect, the propagating modes in the waveguide are converted into radiating modes when they encounter such imperfections. These losses can be reduced by proper choice of materials and the fabrication process. They are the major source of losses in the polymer optical waveguide.

c) Mode conversion losses

These are due to the conversion from the excited mode to other guided modes or radiation modes and are important in situations where the guided mode performs a function, for example, in a directional coupler.

The aforementioned types of losses reduce the available power available at any point in the waveguide and can be described in aggregate as waveguide attenuation. A large number of methods exist to measure the attenuation in optical waveguides.

The two prism method uses a high index prism to couple light into the waveguide by matching the propagation constant of the incident light to the propagation constant of the waveguide modes [29] and another prism to couple light out of the waveguide. The loss is measured by monitoring the change in outcoupled power as a function of distance as the second prism is placed at various positions along the waveguide. This method requires that the prisms be in optical contact with the core so as to maintain the same coupling efficiency. Since the polymer has a concave depression, it will not be possible to couple light as the prism surface will not be in contact with the waveguide core.

Another method of measuring the attenuation is the cut-back method in which the light exiting from the end of the waveguide is monitored at different distances from the input end by progressively cutting back the length of the waveguide. The disadvantage of this method is that the input coupling efficiency has to be maintained and the method is inherently destructive in nature.

A more appropriate technique which we used is a fiber probe technique [30]. In this method, light is coupled into the waveguide and the scattered power is measured as a function of distance. The scattered power is collected by a probe which is usually a large numerical aperture fiber such as a plastic optical fiber. The assumption made in this technique is that the scattered power is proportional to the power propagating in the waveguide. While this is a non-destructive and non-contact method, the loss measurement is difficult when the waveguide has a very low loss (<1 dB/cm). Under these circumstances, the accuracy of measurement depends inversely on the waveguide quality. A variation of the fiber probe method is to use a video camera and microcomputer to capture the streak of light and convert the longitudinal or transverse intensity of the streak into numbers using an analog to digital converter [31]. In the next section, the experimental

setup and procedures for measuring the intrinsic polymer losses and the waveguide losses are described.

3.2 Experimental Setup for Measuring Intrinsic Polymer Losses

It was necessary to have a loss value in dB/cm of the bulk polymer before it was used as a waveguide material. The setup for measuring the losses in the polymer is shown in Fig. 3.1.

The optical adhesive (NOA 61) was sandwiched between two glass microscope slides which were separated by 1.5 mm thick spacers. Care was taken to spread the adhesive uniformly without introducing bubbles. Each glass slide has an area of 7.5 cm x 5 cm and is 0.96 mm in thickness. The sample was cured under a 200 watt mercury lamp for twenty minutes. The polymer-glass sandwich was cut near one end thereby exposing the polymer for launching the laser beam. The cut edge was polished first with a 400 grit followed by 5 μm and 1 μm Al_2O_3. This produced a flat and smooth surface on the polymer which will diverge the laser beam to a minimal extent.

The laser was He-Ne (10 mW, 0.9 mm beam radius, 1.0 mRad beam divergence) emitting at 632.8 nm. A beam-chopper and lock-in amplifier combination was used to minimize noise in the readings caused by stray light. The speed of the chopper is controlled by a chopper controller which also provides a reference signal to the lock-in amplifier. The speed was chosen as 200 rpm so that it did not coincide with harmonics of the 60 Hz a.c power supply. A plastic fiber (core dia. 1 mm, N.A = 0.5) with polished ends picked up scattered light and delivered it to a silicon photodetector (S-1087, Hamamatsu). An amplifier employing a J-FET-input op-amp amplified the signal by a factor of 1000 before it was fed into the lock-in amplifier. The lock-in amplifier gave readings in percentage of power and thus it was necessary to take at least two readings to determine loss in dB/cm. The formula used is

$$\text{loss in dB/cm} = [10 \log_{10} (P_1/P_2)]/d$$

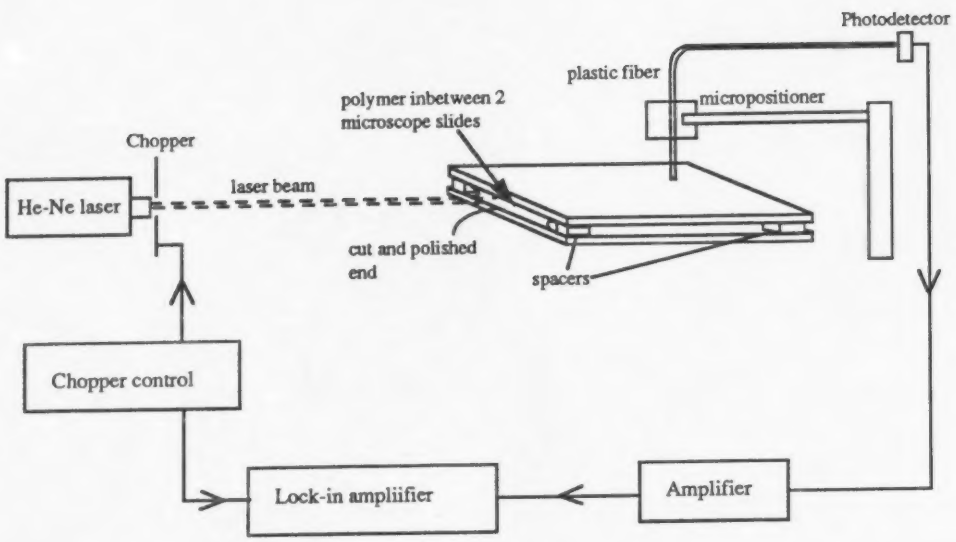

Fig. 3.1 Setup for measuring intrinsic polymer losses

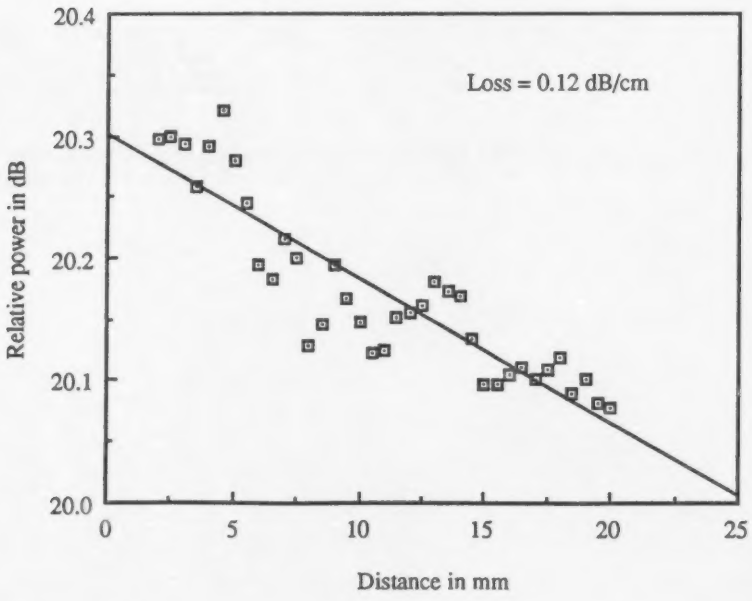

Fig. 3.2 Scattered power from polymer in between microscope slides

where P_1 and P_2 are readings in percentage from the lock-in amplifier and d is the distance between the measurements in centimetres.

The sample was placed on a platform in front of the laser beam such that the beam direction is perpendicular to the polymer surface. The plastic optical fiber was fixed on a micropositioner such that the end of the fiber is 500 μm above the glass surface. The micropositioner and platform were adjusted so that the plastic fiber maintains this distance all along the streak of scattered light and that there was no angular misalignment between the fiber travel and the streak of scattered light. The laser was switched on and the readings were taken from the lock-in amplifier as the fiber traversed along the streak of scattered light. The readings were taken every 0.5 mm for a distance of 18 mm. The graph of the power in dB (arbitrary zero) was plotted as a function of distance as shown in Fig. 3.2. Linear curve fitting of the points gives an average loss of 0.12 dB/cm. This figure indicates that the polymer is a very low-loss material at 632.8 nm. This is an approximate method of measuring the bulk polymer losses because a portion of the power could have propagated in the microscope slides and a small divergence is produced as the laser beam hits the polymer surface. So the actual polymer losses are expected to be < 0.12 dB/cm. The observed loss was verified by measuring scattered power from a different portion of the polymer. The second measurement gave a loss of 0.10 dB/cm indicating the consistency of the losses.

3.3 Experimental Setup for Measuring Waveguide Losses

The method for measuring the losses in the polymer optical waveguide is similar to that explained in the previous section. The setup is shown in Fig. 3.3. Instead of coupling the beam directly into the waveguide, a lens first coupled the light from the laser into a multimode optical fiber. The distance between the fiber and the lens was adjusted precisely using micropositioners for the lens and the fiber. The other end of the fiber was mounted in a fiber holder on a micropositioner and was butt-coupled to the optical waveguide. The

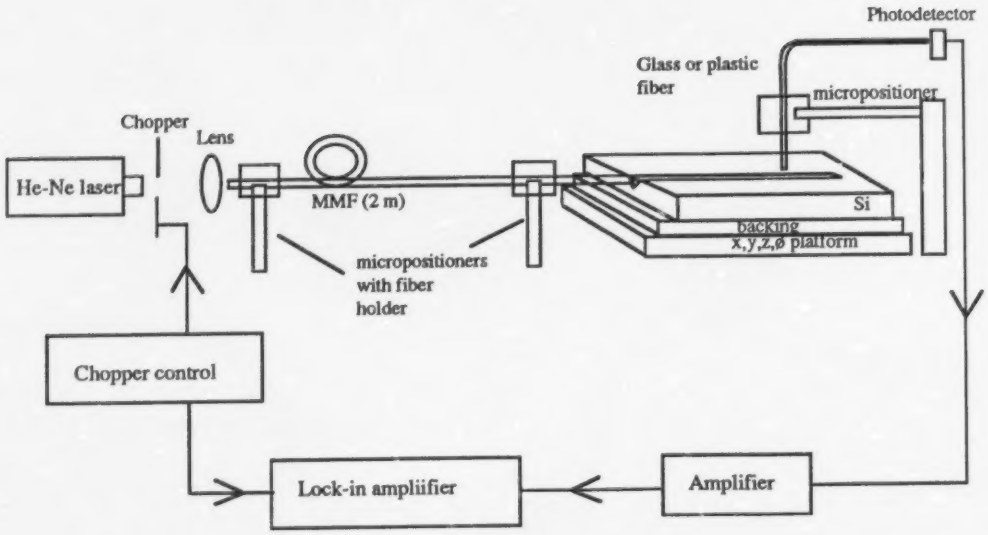

Fig. 3.3 Setup for measuring losses in waveguides

input end of the waveguide was polished as described in the previous chapter. The silicon piece containing the optical waveguide was mounted with epoxy on a firm backing such as PCB board to give it more strength. The PCB substrate is epoxied to a level platform. Before the fiber probe was placed over the waveguide, it was necessary to align the travel of the fiber probe precisely with respect to the waveguide to eliminate errors in measurements. The technique by which this was done is given is in Appendix F.

A microscope was used to position the end of the fiber precisely against the waveguide. Final adjustments with the micropositioner for improving coupling efficiency were done by maximizing the light emanating from the end facet of the waveguide. The fiber probe was placed at a distance of 1.05 mm away from the waveguide surface in the case of a MM glass fiber and 500 μm in the case of a plastic fiber. Placing the fiber a slight distance away from the waveguide surface helps in capturing more scattered light and also smooths the scattered power fluctuations caused by inconsistencies in the waveguide roughness. The laser was switched on and the lock-in amplifier parameters were adjusted to get a suitable range in readings and also to prevent overloading of the amplifier.

Scattered power was measured as a function of distance along the waveguide. The spacing of each reading was 0.5 mm.

3.4 Loss Results for Polymer Waveguides

The results obtained for the various loss measurements are given in two sub-sections: a) losses in waveguides made by grinding and polishing b) losses in waveguides made by doctorblading. In the first subsection, experiments were done with different buffer layer thicknesses. In the second subsection, experiments were done with aluminum and SiO_2 buffer layers.

3.4.1 Losses in waveguides made by grinding and polishing

As mentioned in the second chapter, it was necessary to have a buffer layer between the silicon substrate and the polymer core region to prevent refraction of the light into the substrate. Because the deposition rate of CVD oxide is slow, the buffer deposition is a significant cost factor in waveguide fabrication. As part of the research, we have experimented with different thicknesses of the buffer layer to determine the minimum thickness required.

The first graph (Fig. 3.4) shows the scattered power from a waveguide having no buffer layer. Here it is to be expected that the light will be attenuated heavily in the waveguide. The loss measured was 47.4 dB/cm. The scattered power intensity dropped to the noise level within 4 mm from the coupling end. Fig. 3.5 shows the scattered power from a waveguide with a 0.6 μm SiO_2 buffer layer. The loss from this waveguide was measured at 13.5 dB/cm. Fig. 3.6 shows that the loss in a waveguide with 1 μm buffer layer is 8.7 dB/cm. The scattered power from a waveguide with 2 μm SiO_2 is shown in Fig. 3.7. and the loss is 3.3 dB/cm. In a waveguide with 3 μm thick SiO_2 layer, the loss measured was 3.7 dB/cm (Fig. 3.8). The loss appears to have increased with an increase in the buffer layer thickness. This means that the losses are no longer determined by increases

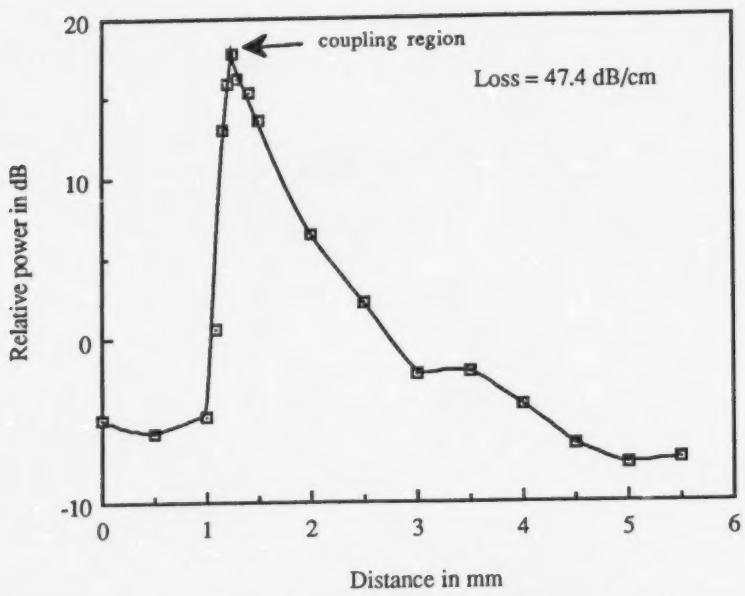

Fig. 3.4 Scattered power from waveguide with no buffer layer

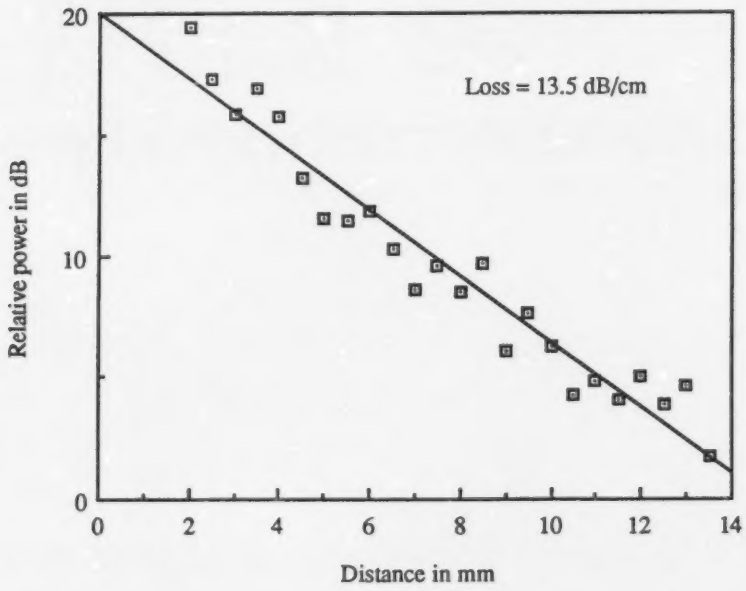

Fig. 3.5 Scattered power from waveguide with 0.6 μm SiO_2 buffer layer

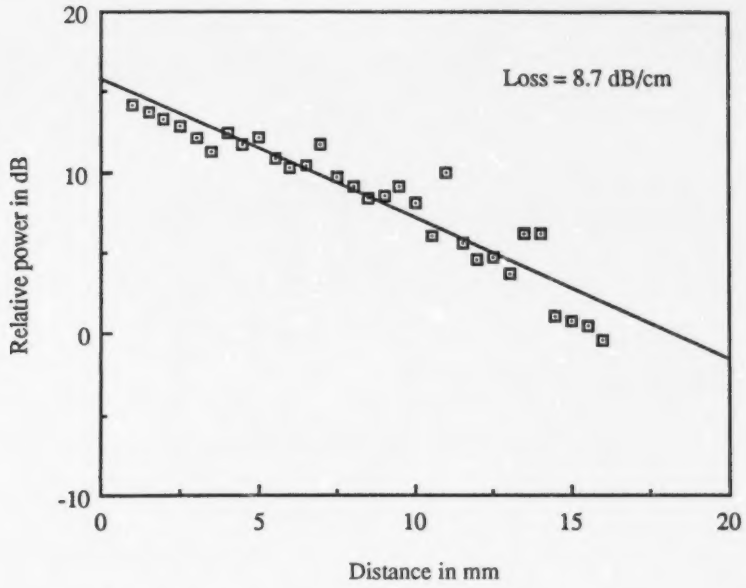

Fig. 3.6 Scattered power from waveguide with 1 μm SiO_2 buffer layer

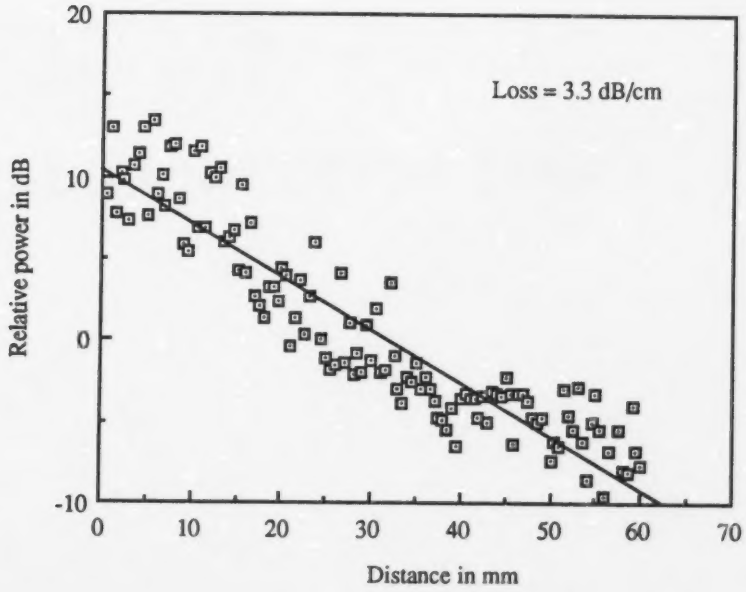

Fig. 3.7 Scattered power from waveguide with 2 μm SiO_2 buffer layer

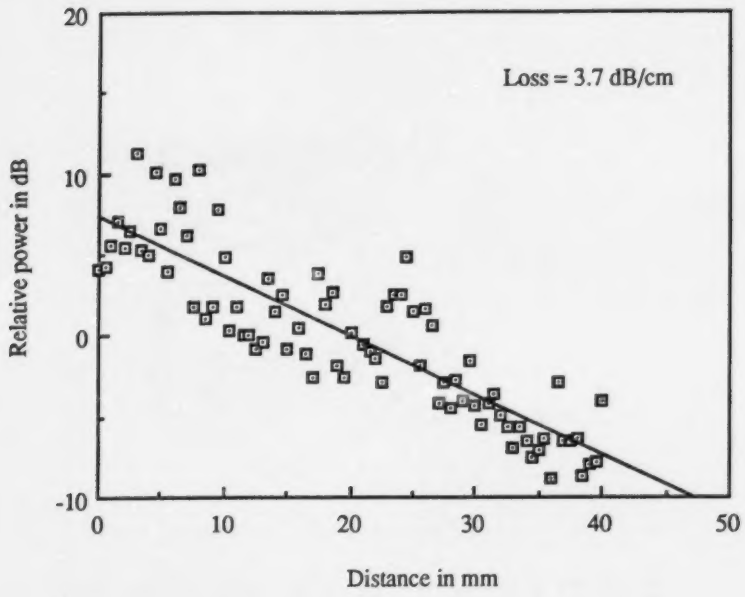

Fig. 3.8 Scattered power from waveguide with 3 μm SiO_2 buffer layer

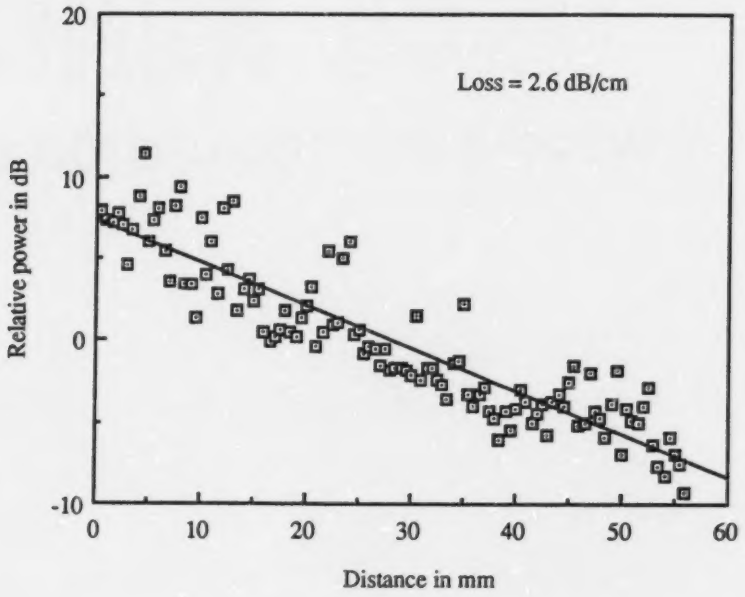

Fig. 3.9 Scattered power from waveguide with 2 μm SiO_2 buffer layer and upper cladding layer

in the buffer layer thicknesses, but are more dependent on the surface roughness of the waveguides. It will be noticed from these plots that the fluctuations in the scattered power increase with decreasing losses in the waveguide. Thus a certain amount of inaccuracy is introduced as the losses drop to low values (the uncertainty in the loss is estimated to be +/- 1.25 dB/cm for the measurement of Fig. 3.8) and at this time the fluctuations of scattered power indicate the inconsistencies in surface roughness brought about by the fabrication process. To reduce the loss due to surface roughness on these waveguides, a refractive index fluid of index 1.53 was dispensed uniformly over the waveguide with the lowest loss measured. Scattered power measurements done on this waveguide indicate a loss of 2.6 dB/cm (Fig. 3.9). This is a drop of around 0.7 dB/cm. Since our loss requirement is < 1 dB/cm, we looked at other ways of fabricating these polymer waveguides. The losses in waveguides made by doctorblading are discussed in the next section.

3.4.2 Losses in waveguides made by doctorblading

In this method of making waveguides, the polymer surface is untouched by the abrasive during excess polymer removal except at the top edges. While this creates a waveguide with a very smooth surface which decreases the losses, it becomes more difficult to measure the losses accurately. The scattered power measurement of one such waveguide with about 2.6 μm buffer layer is shown in Fig. 3.10. The curve fit indicates an average loss of 0.5 dB/cm. The fluctuations seen on the graph are due to the roughness on the waveguide upper edges created during excess polymer removal. To verify the low loss, another measurement was made on another waveguide sample. The curve fit on the data indicates a loss of 1.6 dB/cm (Fig. 3.11). Due to the wide fluctuations seen on the graph (a maximum difference of 18 dB over 4.5 cm), it would be inappropriate to say that there is a large difference in losses between that shown in Fig. 3.10 and this graph. Using a microscope to observe the surface of the waveguide into which light was coupled from a He-Ne laser beam, we could see two streaks of light on the edges of the waveguide which

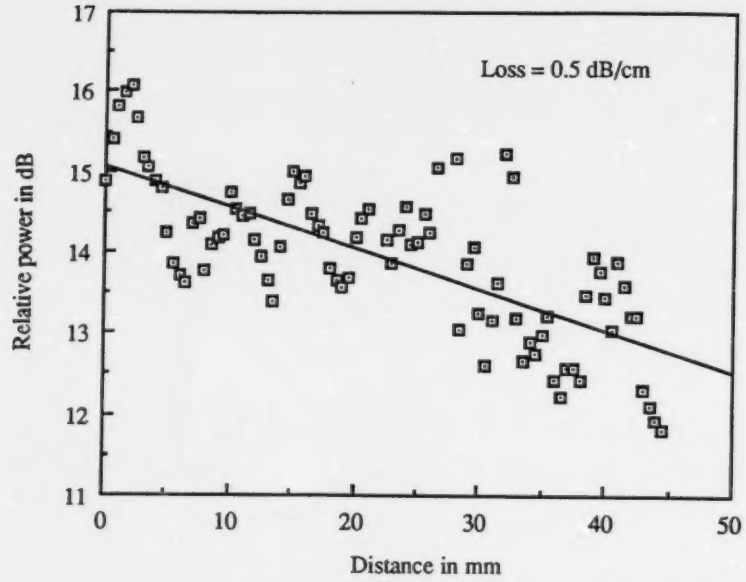

Fig. 3.10 Scattered power from waveguide with 2.6 μm SiO_2 buffer layer (doctorbladed core material)

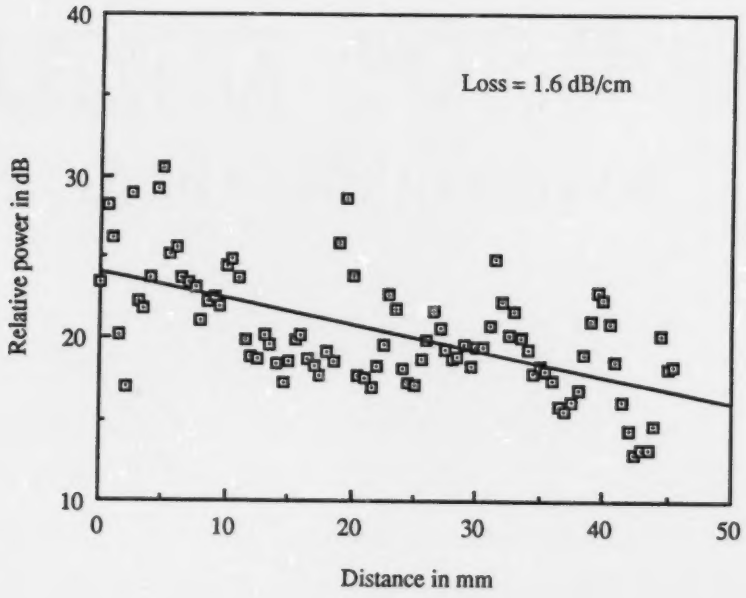

Fig. 3.11 Scattered power from waveguide with 3 μm SiO_2 buffer layer (doctorbladed core material)

had a higher intensity than the scattering centres in the bulk of the polymer waveguide. These are scattering points generated during the removal of excess polymer. Since the scattered power now becomes more a function of the edge roughness caused by the polishing than a function of the power in the waveguide, a more accurate loss measurement technique is required for these low-loss waveguides, but has not yet been devised.

For increasing the reflectivity of taps, we must deposit Al on them. It would be easier to deposit Al everywhere on the waveguide so that a special process would not be required for selective deposition. The side-scattered power from a waveguide with Al deposited on SiO_2 buffer layer is shown in Fig. 3.12. The measured loss was 2.4 dB/cm. This loss is similar to that in a waveguide with Al alone and no SiO_2 buffer layer (2.3 dB/cm). There is a very steep slope near the coupling end of the waveguide for the first 5.5 mm with a loss of 34.6 dB/cm. The steep slope is due to the attenuation of higher order modes that hit the metal walls at larger angles for which the reflectivity is smaller and the number of bounces per unit length is greater. Since the loss is high in the aluminized waveguide, a special method of selectively coating the taps was developed as described in Chapter 2.

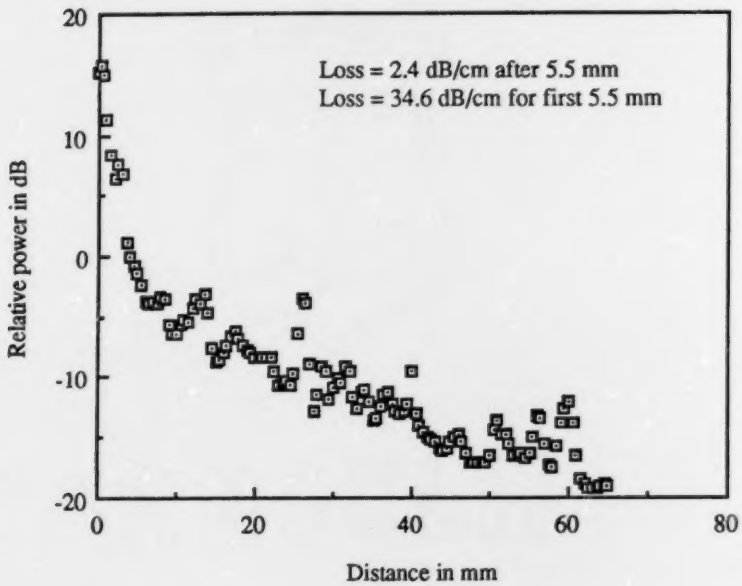

Fig. 3.12 Scattered power from waveguide with Al on 3 μm SiO_2 buffer layer (doctorbladed core material)

CHAPTER 4

WAVEGUIDE TAPS AND FIBER SELF-ALIGNMENT

4.1 Introduction

Waveguide taps are beam splitters in which a portion of the power propagating in the waveguide is accessed without disturbing the direction of propagation of the main beam. Two types of beam splitters have been previously demonstrated using grooves etched in silicon. In the first, glass channel waveguides were formed with sidewall notches which split an incoming beam into two orthogonal waveguides and the amount of splitting was controlled by the size of the notch [14]. In the other, thin film beam splitters were employed wherein a v-groove waveguide acts as an optical perturbation in the beam path to cause partial reflection and transmission [32]. In our beam splitter, sidewall taps to tap a portion of the light out of the plane of propagation for coupling into surface mounted devices are fabricated in the channel waveguides using silicon micromachining [33]. The micromachining of the sidewall taps depends on a phenomenon called undercutting which will be explained in the next section. In later sections, we shall describe how this undercutting was utilized for fabricating two types of taps. Finally the design, fabrication and testing of a 12x12 tapping array is explained along with a demonstration of fiber to waveguide coupling using alignment grooves.

4.2 Undercutting Phenomenon at Corners

Undercutting is the phenomenon where the etchant removes etchable material underneath the mask. A prominent location where undercutting takes place is at outside

(convex) corners in (100) oriented silicon wafers during anisotropic etching. The effect of the undercutting is beveled surfaces at the corner. Corner undercutting does not occur at inside (concave) corners. Undercutting is significant in dielectric isolation techniques of integrated circuits where it is a limitation to the useful surface area when deep etching is used [34]. To overcome the undercutting at corners, compensation patterns can be added to the mask so that as soon as the etching reaches the required depth, the corner under the compensation pattern reaches the main mesa tip [34]. Fig. 4.1 shows the different facets which result due to the undercutting at a 90° corner in the mask. The etching is done in EPW at 115°C. Because of the undercutting, there are two (212) planes which meet at the corner of the mesa. The (212) plane intersects the (100) surface at 48.2° and its trace makes an angle of 18.4° with the (111) trace [34]. The (212) planes meet the usual (111) plane at the side wall on either side of the mask corner. If the mask edge is not properly aligned to the wafer flat, then instead of the smooth (111) sidewall planes, striated planes will occur and the (212) planes will be asymmetrical.

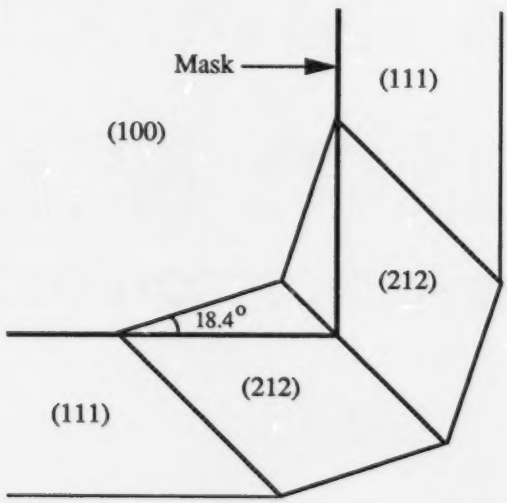

Fig. 4.1 Facets at an undercut corner

4.3 Types of Taps

Two types of taps can be made which utilize the phenomenon of corner undercutting. They are

a) Outside taps

In this type of tap, a rectangular hole is made in the etch window meant for the straight waveguide (Fig. 4.2 (a)). Each rectangular hole will form a tap after the anisotropic etching. The corner undercutting will create a rounded surface at both 90° corners which will be bounded by the (212) planes (Fig. 4.2 (b)). Light propagating in the waveguide will spread as it comes to the opening and will hit one of the (212) planes and be deflected upwards. The remaining light will be reflected upwards from the end facet of the waveguide which acts as a 100% tap. The disadvantage of the outside tap is that a portion of the light will be lost as it will hit the other (212) plane at a small angle and will be not be deflected onto the photodetector. Apart from taking more space on the wafer than the inside tap, these taps are also expected to be mode sensitive, that is the amount of tapping would depend on the distribution of angles of the rays at the tap opening.

b) Inside taps

In the case of inside taps, rectangular mask projections are made in the etch window meant for the waveguide (Fig. 4.3 (a)). After etching, a sidewall tap will be formed bounded by two (212) planes and an inner sidewall (Fig. 4.3 (b)). Light propagating in the waveguide will hit the obstructing (212) plane and will be deflected upwards at about 20° from the normal. A larger angle of about 30° from the normal will result above the air interface due to refraction (Fig. 4.4). This method of tapping is better as the tapping structure is confined within the waveguide. It is also possible to design these taps to control the percentage of light being tapped. Looking from one end of the

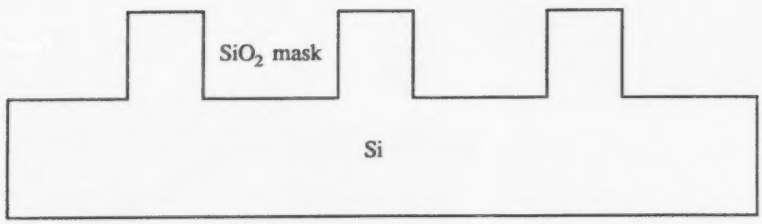

Fig. 4.2 (a) Etch window for waveguide with three outside taps

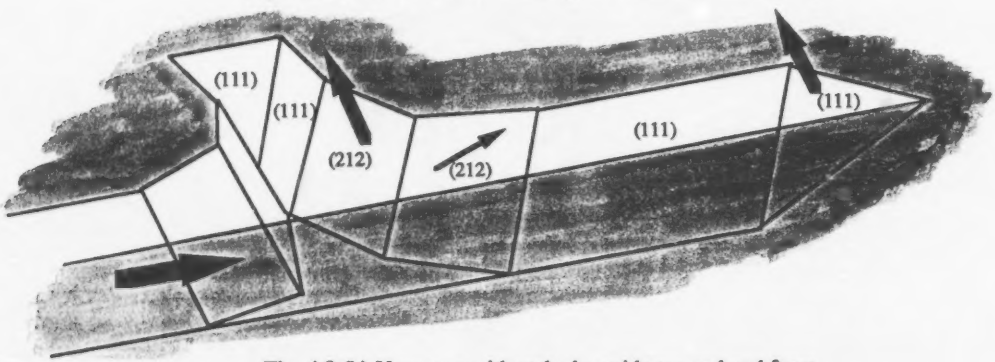

Fig. 4.2 (b) V-groove with etched outside tap and end facet

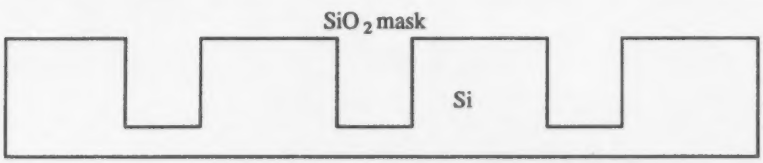

Fig. 4.3 (a) Etch window for waveguide with three inside taps

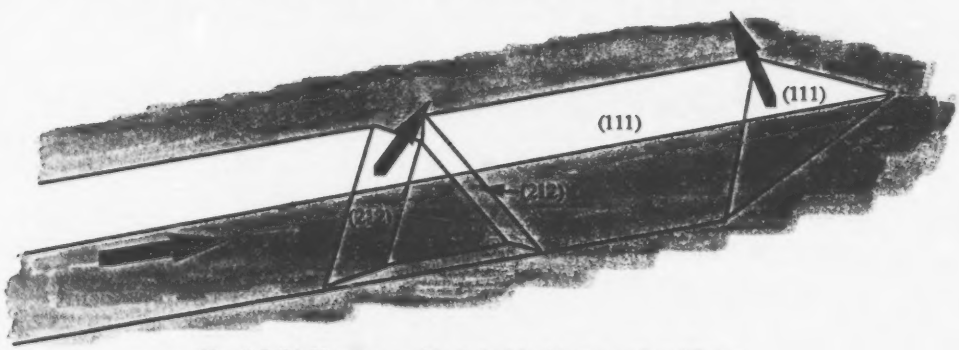

Fig. 4.3 (b) V-groove with etched inside tap and end facet

waveguide, the (212) plane will present an obstruction to the propagating light (Fig. 4.4). By controlling the size of the tap, the percentage of light tapped can be controlled.

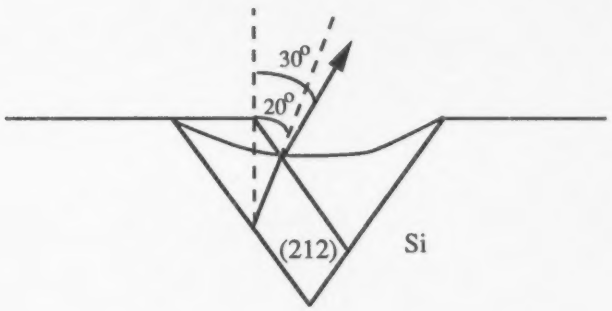

Fig. 4.4 View of inside tap from end of waveguide groove

4.4 Etching Profiles of Rectangular Masks

A rectangular mask as shown in Fig. 4.5 (a) is used to get the three dimensional sidewall tapping structure that can tap light out-of-plane. It consists of two 90° corners which will be undercut during the anisotropic etching. The etching will proceed as indicated by the dotted lines on the mask. At point a, undercutting has begun at both the corners, but there is a (111) sidewall between the corners. At point b, the inner (212) planes have met reducing the previously trapezoidal shape of the (111) plane to a triangular shape. This triangle will get smaller and smaller until it finally disappears. The (111) planes at either side of the rectangular mask will also disappear as the (212) plane extends towards the waveguide edge. At point P which is the intersection of the two (212)-(212) corners, the inner (212) planes disappear at the mask surface leaving only the outer (212) planes. One of the remaining outer (212) planes will be used for tapping the light onto a photodetector. The inner sidewall can be rough at times depending on the etching, but will be insignificant in scattering light because light will strike the rough surface at a glancing angle. The mask dimensions are designed such that the (212)-(212) corners reaches the point P at the same time the v-groove is etched completely.

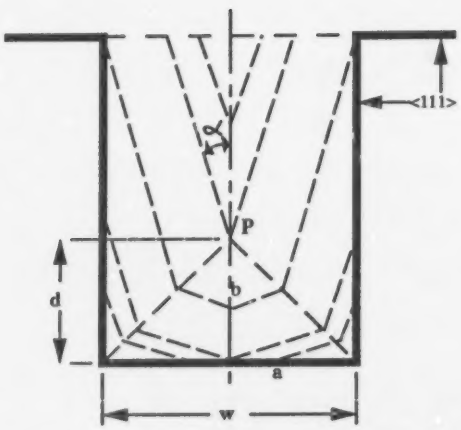

(a) Successive etching shapes with a rectangular mask. (α= 18.4°)

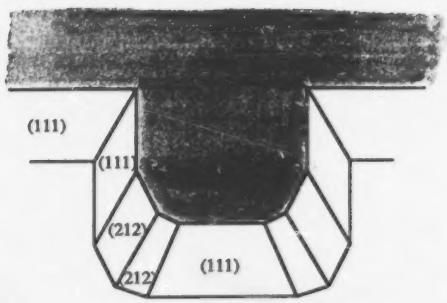

(b) Etched shape at point a

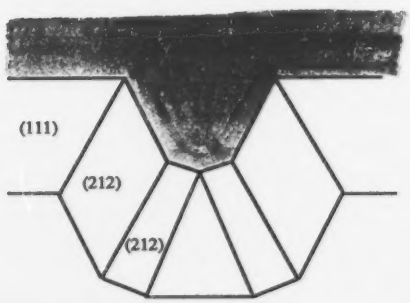

(c) Etched shape at point b

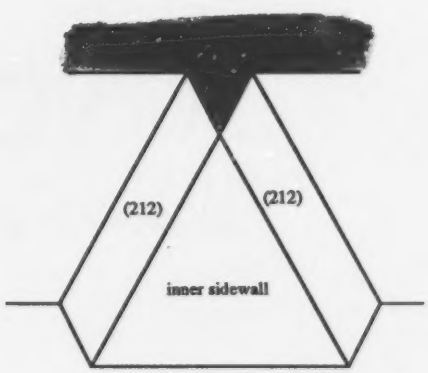

(d) Etched shape at point P

Fig. 4.5

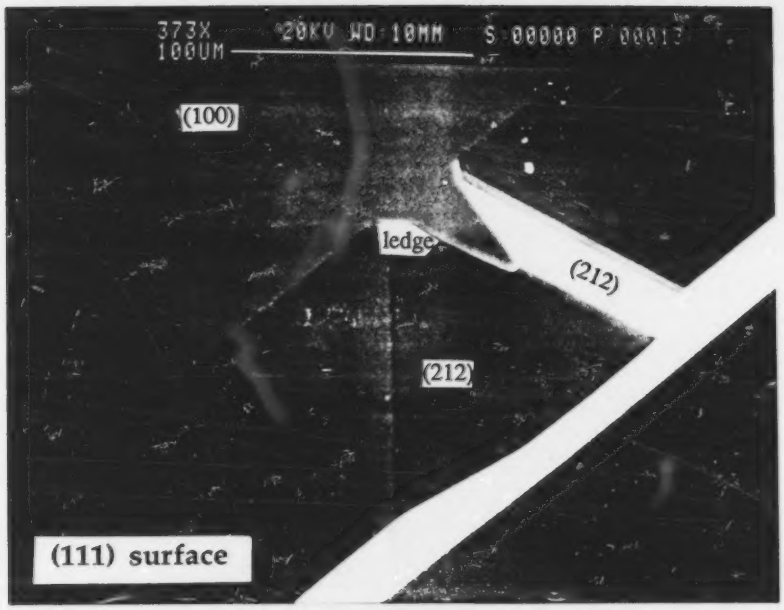

Fig. 4.6 (a) Photograph of inside tap with etching stopped at point P

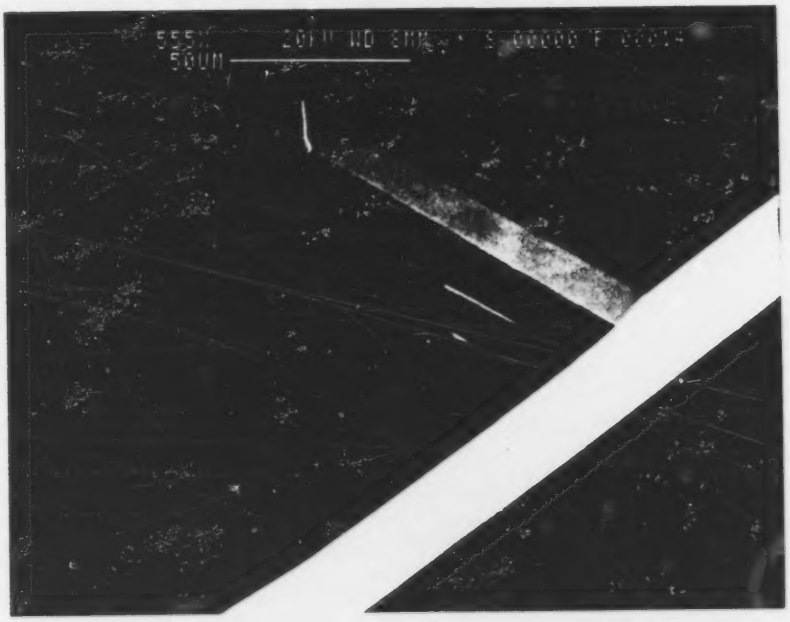

Fig. 4.6 (b) Photograph of inside tap with etching continued beyond P

Fig. 4.6 (a) shows a SEM picture of an inside tap where etching has been stopped at point P. There appears to be a small ledge on the top surface of the tap and we speculate that this could be the ($\bar{3}23$) plane [34]. Fig. 4.6 (b) shows a SEM picture of an inside tap where etching has proceeded well beyond P leaving a rough surface on the inner wall.

4.5 Calculation of Attenuation in Waveguide with Three Inside Taps and One End Facet

A waveguide was fabricated with three inside taps and one end facet. The three inside taps were of the same size. Light from a He-Ne laser was coupled into the waveguide and the scattered light from the waveguide surface was picked up by a plastic optical fiber. Fig. 4.7 shows the result obtained. There is a consistent drop of around 2 dB from one inside tap to the next attesting to the fact that the equal size taps tap an equal proportion of the power propagating in the waveguide. The end facet taps a different amount of power because it taps out all the remaining light in the waveguide.

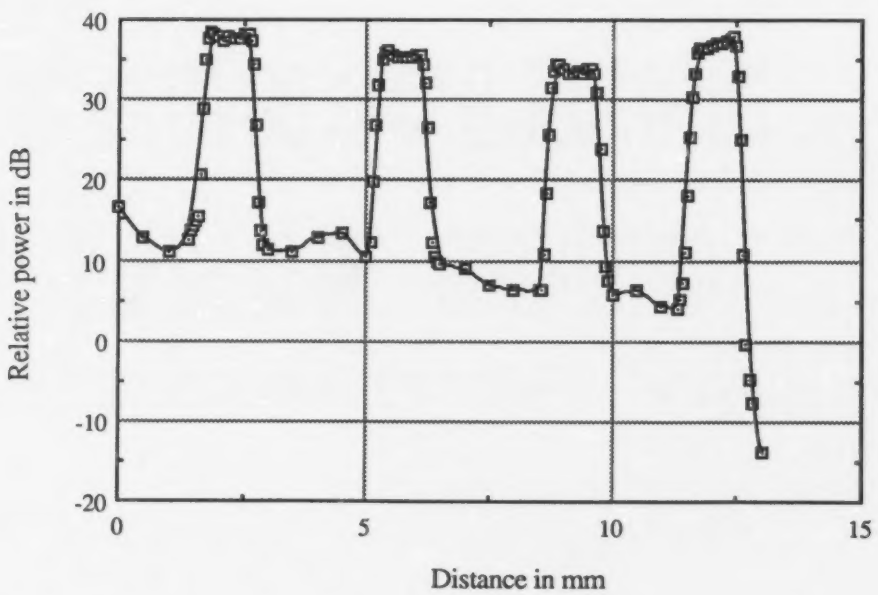

Fig. 4.7 Scattered power from waveguide with three inside taps and one end facet

Let P_1, P_2 and P_E be the relative power tapped from the second tap, third tap and end facet respectively. From Fig. 4.7, $P_1(dB) = 35.5$ dB, $P_2(dB) = 33.7$ dB and $P_E(dB) = 36.9$ dB. We can then write:

$$P_E/P_2 = [(1-T)/T]\ 10^{-(\hat{\alpha}/10)x}. \quad (1)$$

$$P_2/P_1 = (1-T)\ 10^{-(\hat{\alpha}/10)x}. \quad (2)$$

where T is the tapping ratio for each inside tap, $\hat{\alpha}$ is the attenuation in dB/cm of the waveguide between the taps and x is the distance between each tap (0.35 cm). From the above equations,

$$T = P_2^2/(P_1P_E).$$

or $10 \log T = 2P_2(dB) - P_1(dB) - P_E(dB) = -5$ dB.

Therefore $T = 10^{-0.5} = 0.32$ which gives a 32 % tapping ratio for each inside tap. From equation (2),

$$\hat{\alpha} = (1/x)[P_1(dB) - P_2(dB) + 10 \log(1-T)]. \quad (3)$$

Substitution of the values yields $\hat{\alpha} = 0.4$ dB/cm. This is only an average value which has a large uncertainty because of the +/- 0.5 dB uncertainty in the values of $P_1(dB)$, $P_2(dB)$ and $P_E(dB)$.

4.6 Design of Inside Taps

As mentioned before, it is possible to have different tapping ratios by varying the size of the inside taps. To have serial taps which tap out the same amount of power in a waveguide, the tapping ratio will not be the same for each tap since the power available in the waveguide decreases due to the tapping. The tap size must therefore increase as the light propagates towards the end facet of the waveguide. Fig. 4.8 shows the tap as viewed from the waveguide cross-section. The inner sidewall of the tap is nearly parallel to the (111) sidewall and can be taken as a side of the smaller triangle. Let A_n be the area of the n^{th} tap as seen from the end of the waveguide and A_{tot} be the cross-sectional area of the

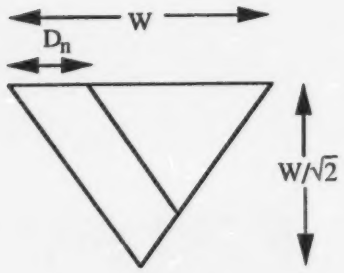

Fig. 4.8 Cross-sectional view of waveguide with tap

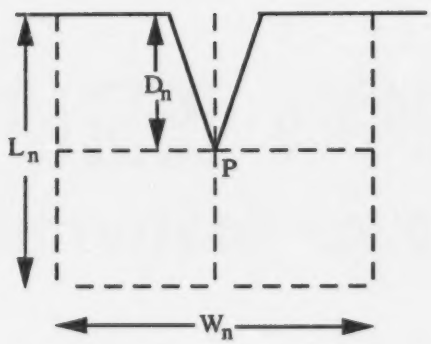

Fig. 4.9 Construction of rectangular mask for given D_n

waveguide. Then assuming that the optical beam has a uniform intensity in the waveguide, we can say that

Fraction of power tapped = A_n/A_{tot}

The value of A_n is controlled by D_n which is the length of the tap projection. We can derive the relation (See Appendix G) between the size D_n and the tap number as

$$D_n = W[\,1- \sqrt{(N-n)/(N-n+1)}\,] \qquad (4)$$

where W= width of the waveguide

N= total number of taps in the waveguide

n= tap number

Hence for a waveguide with 4 taps and W= 125 μm, the value of D_n for each tap is:

D_1= 16.75 μm, D_2= 22.94 μm, D_3= 36.61 μm, D_4= 125 μm (end facet)

The value D_n gives the distance from the waveguide edge at which the etching should stop for each tap. From our knowledge of the etching in rectangular masks, we know that this point should coincide with the disappearance of the extra (212) planes, that is point P, to get a well-defined tap with an inner sidewall. Also point P is the point up to which the etching can be monitored comfortably, because after point P, the tip of the tap recedes at ~ 8 times faster than the tip before point P. If we know the etch rate of the (212)-(212) corners and the etch rate in the <100> direction, we can put an appropriate size of square mask on either side of point P as shown in Fig. 4.9 so that as soon as the silicon underneath these squares disappear to reach point P, the etching of the v-groove is complete. The etch rate of the (212)-(212) corner has been found to be 0.35 μm/min with a variation of +/- 7% (See Appendix H for method of determining etch rate). The etch rate in the <100> direction was found to be 0.64 μm/min for a fresh EPW solution. This rate increases with age of the solution to as high as 1.3 μm/min for a one-day-old solution. The etch rate of the (212)-(212) corner was not affected by the increase in the <100> etch rate. To etch a v-groove that is 125 μm wide or 88.4 μm deep, the etch time required

would be 138 minutes. The same time should be taken by the undercutting of the rectangular mask to reach point P. The diagonal of the square required is 0.35 x 138= 48.3 μm. This would give a side of sin(45) x 48.3 = 34.2 μm. Now the length L_1 and width W_1 of the mask required for tap 1 are given by

$$L_1 = D_1 + 34.2 \sim 51\ \mu m$$

$$W_1 = 2 \times 34.2 \sim 68\ \mu m$$

4.7 A 12 x 12 Tapping Array for a Hybrid Integrated Optoelectronic Switch Matrix

For a 12 x 12 tapping array, there will be twelve waveguides, each waveguide having twelve taps. Out of these twelve taps, eleven will be inside taps and the twelfth one will be the end facet. The waveguides are on 250 μm centres so that the tapping array is compatible with standard fiber ribbon cable. Alignment grooves which are larger than the waveguide grooves are provided before the waveguides so that fibers can couple light with support.

4.7.1 Design of tapping array and alignment grooves

The width of the alignment groove and the width of the waveguide groove depend on the fiber cladding and core diameters and are calculated as shown in Appendix I. The core of the fiber is completely covered by the cross-sectional area of the waveguide. It is not necessary to etch the alignment groove fully, only the depth to which the fiber extends in the v-groove. The sizes of the tap (D_n) are determined by using N as 12 in equation 4. The appropriate size squares are added to each D_n to give the dimensions of each of the rectangular masks.

A separation of 20 μm is introduced between the two etch windows so that a saw cut can be made to remove the intermediate silicon (see Section 4.8). The fiber can then be made to butt against the waveguide. A waveguide distance of 2.5 mm is introduced before the first tap so that any mode coupling loss would be removed in this distance.

4.7.2 Fabrication of the array

The photolithography and anisotropic etching are carried out first on a wafer. During anisotropic etching, it is necessary to constantly check the sample towards the end of the etching process so that it can be removed at the right time. Sometimes due to inconsistent etch rates, the sample may become over-etched and the taps sizes will be too small. A SEM picture of an etched tapping array is shown in Fig. 4.10. Due to the small dimensions of the tapping array and the large number of taps present, it is convenient to coat all the taps with Al including the tap-free areas. It would be time consuming to utilize negative resist lithography and expose each of the 144 taps individually using the microscope objective as described in Section 2.3.4. The deposition of Al makes it unnecessary to deposit a layer of CVD oxide on the silicon surface as the effect would be the same. The optical adhesive is doctorbladed on and cured. The excess polymer is removed by polishing. Since we are able to test only one waveguide at a time with its 12 taps by butt-coupling with a single fiber, the alignment grooves are unnecessary. The ends of the waveguides are polished before end firing with a single fiber. In the OEIC switch matrix application, the input to the tapping array will be 12 fibers from 12 lasers which will require the use of the alignment grooves. The steps required for making a fiber to waveguide coupling using the alignment grooves are described in the next section.

4.7.3 Testing of a waveguide with 12 taps

The tapping array is mounted on the platform and its rotation stage is rotated by 31.4^{o} so that the light from the inside taps exit vertically upwards. Light from each tap is picked up by a MM glass fiber. The fiber position is adjusted so that it nearly touches the taps and it picks up the maximum light. The readings are taken from the lock-in amplifier for each tap location.

Fig. 4.11 shows the graph of relative power in dB for each of the 12 taps. The power from the 12^{th} tap is very low because of the different angle at which light exits

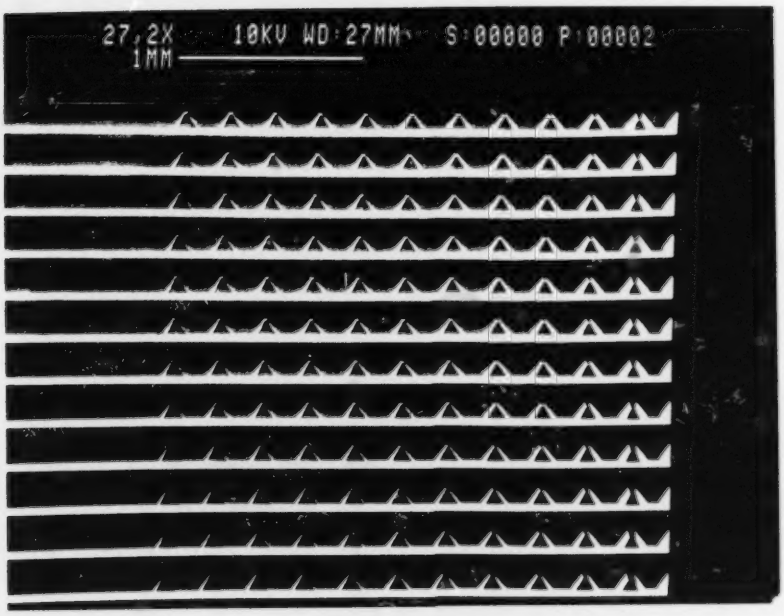

Fig. 4.10 SEM photograph of the top view of tapping array after EPW etching

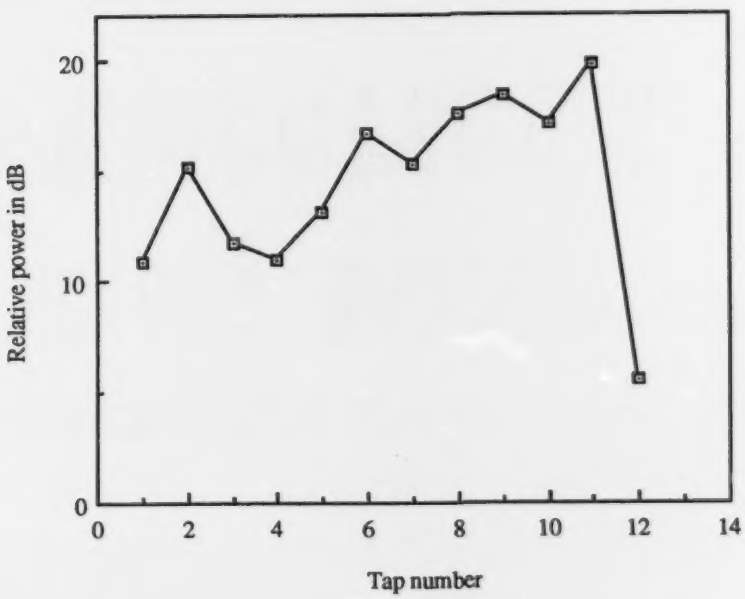

Fig. 4.11 Results of tap measurements

from the end facet. The trend is towards increasing tapped power as one goes towards the end facet. There is a maximum difference of about 9 dB in the power from the inside taps. The reasons for the observed non-uniformity in the tapped power could be many :

(1) The fiber probe may not be picking up all the light from each tap.

(2) The designed size of the taps did not take into account the depression in the polymer.

(3) The simplified description of the etching of a rectangular mask given in Section 4.4 did not consider the occasional presence of an interface plane at either side of the taps. This plane makes an angle of about 45º with the trace of the (111) plane and is prominent in small-sized and medium-sized taps (See Fig. 4.12). Calculations indicate that it could be a (011) plane. Fig. 4.12 (a) shows a small-sized tap which has been slightly over-etched. Fig. 4.12 (b) shows a medium-sized tap which has not been etched fully. The reason for the occurrence of this extra plane needs to be investigated further.

(4) There could be modal effects coming into play which will lead to different results for different coupling conditions. However, this effect can be reduced by using the light from a LED.

(5) There could be air-pockets under the polymer near each tap.

4.8 Demonstration of Fiber to Waveguide Coupling using Alignment Grooves

As mentioned in Section 4.7, alignment grooves are provided near the waveguides so that fibers can sit in them and couple light into the waveguides. Due to the geometry of the groove, a fiber has no lateral movement and if the waveguide core matches the fiber core, then an efficient means of coupling with self-alignment is achieved. The view of the alignment groove and the waveguide groove after waveguide fabrication is shown in Fig. 4.13 (a). A saw cut is made between the two grooves to remove the intermediate silicon so that the fiber can butt tightly against the polymer waveguide (Fig. 4.13 (b)). The fiber is stripped of its jacket and cleaved to the appropriate length. To have a good coupling

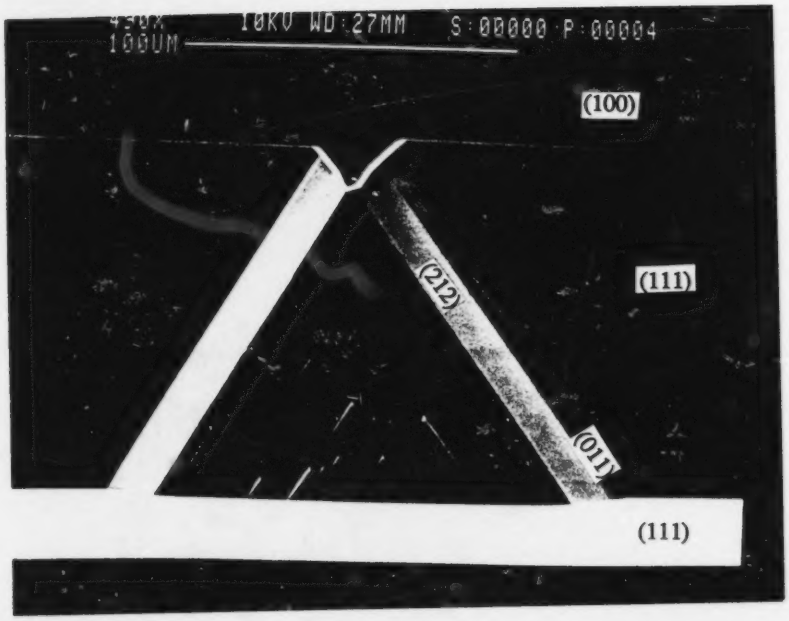

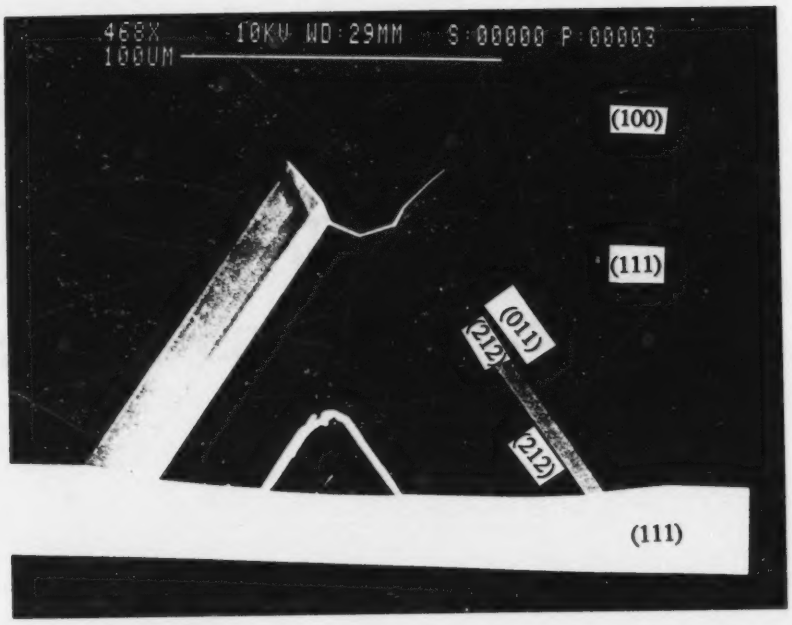

Fig. 4.12 Pictures of taps showing the presence of an interface plane

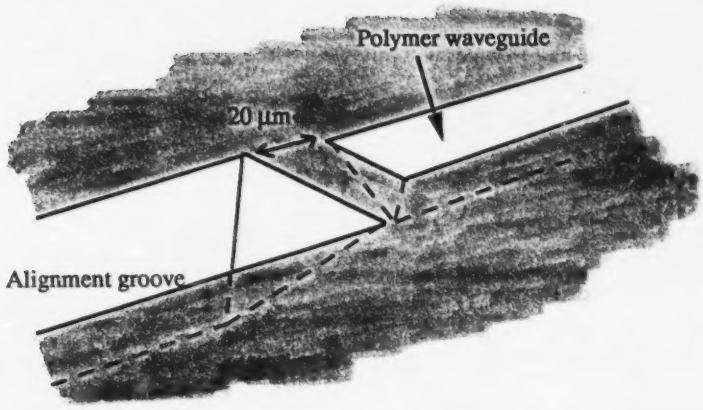

Fig. 4.13 (a) Schematic of alignment groove and waveguide

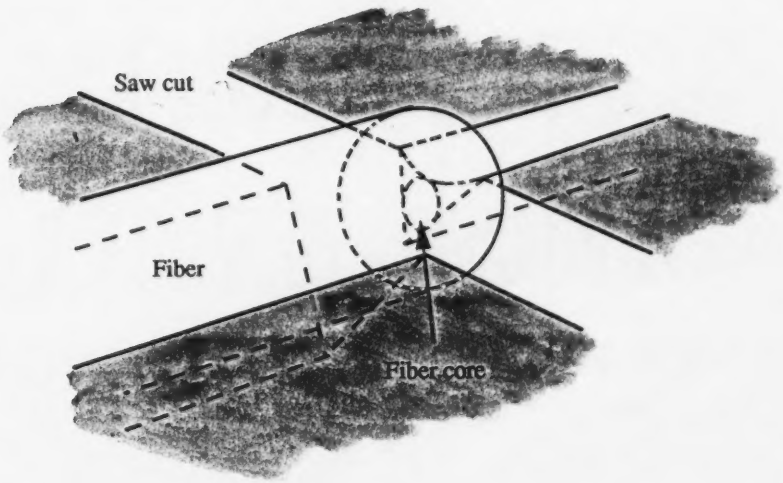

Fig. 4.13 (b) Fiber assembled in alignment groove
after making a saw cut to remove the intermediate silicon

efficiency between the fiber and the polymer waveguide, the fiber ends must be flat and smooth.

4.8.1 Fabrication process

To measure the coupling efficiency of the fiber alignment, the tapping array is over-etched so that all the taps disappear. The wafer containing the v-grooves is deposited with about 3 μm of CVD SiO_2 to act as buffer layer. The wafer is next shadow-masked with a cover slip to selectively deposit the aluminum on the end facet. This is done by placing the edge of the cover slip about 100 to 200 μm from the end facets of the waveguide grooves while covering all other areas of the grooves. The wafer and cover slips are clamped on the target plate and mounted in the vacuum chamber. A ~0.1 μm thick layer of Al is then grown.

Next, a straight edge tape is placed on the alignment grooves so that optical adhesive will not be deposited in them during the deposition of the adhesive in the waveguide grooves. It is necessary that no gaps exist underneath the tape as optical adhesive will ooze through during the doctorblading action. This can be ensured by placing the tape slightly into the waveguide grooves (about 125 μm). Optical adhesive is next doctorbladed onto the waveguides. The adhesive is cured and the excess polymer is polished off. The masking tape is removed and the grooves are inspected to see if the mask was effective.

The next step in the fabrication process is to remove the intermediate silicon between the alignment grooves and the waveguides. This is done with a wafer saw. The thickness of the wafer is measured with a micrometer. The thickness will not be uniform because of the uneven layer of crystal bond underneath the wafer from the mounting of the wafer on the polishing holder. The average thickness is determined and 100 μm is subtracted from it. This will give the height of the cut assuming a depth of cut of 175 μm and the tape thickness of 75 μm. The number of cuts required will depend on the distance

between the end of alignment groove and the start of waveguide polymer. Because of the masking action of the tape during application of polymer, this distance will not always be consistent. It may take 4 or even 5 cuts to remove the unwanted areas. The polymer surface at the cut is quite smooth considering the large grit on the blade.

4.8.2 Assembly of fiber in alignment groove

The silicon sample is mounted on a platform. A fiber that is stripped of its jacket and cleaved to a length of at least 6 mm is clamped in a fiber holder sitting on a micropositioner. Small amounts of "five minute epoxy" are applied to the alignment groove where the fiber is to be placed. The epoxy will start running into the v-grooves and will be used to hold the fiber rigidly in place. The alignment grooves are brought underneath the fiber and the micropositioner is adjusted so that the fiber sits in the alignment groove. A knife edge is brought down on the fiber at the same time as back and forth movements of the fibers in the grooves are made. As the knife edge touches the fiber it will be harder to slide the fiber in the groove. The fiber should butt against the polymer waveguide without pressure. At this point the blade is lowered enough so that the fibers do not move. The epoxy is allowed to cure and the knife edge is removed. Fig. 4.14 (a) and (b) shows SEM pictures of a single fiber assembled in the alignment groove.

4.8.3 Loss measurements

The losses were measured using a single fiber not epoxied in the groove. The length of the fiber should be at least 2 metres so that there will be a reduced number of cladding modes at the end of the fiber. First a silicon detector (S1133, Hamamatsu) is mounted in front of the fiber and its relative position adjusted for maximum power reading in the lock-in amplifier (reading P_1 which is the power that will exit from the fiber in the coupling to the waveguide). Next the silicon sample is placed securely on a platform and the fiber is tilted and placed in the alignment v-groove. When the fiber

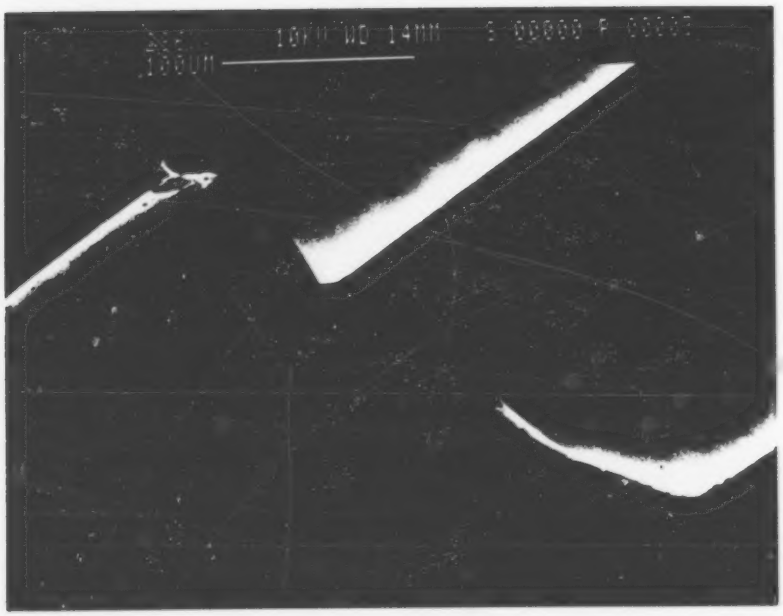

(a)

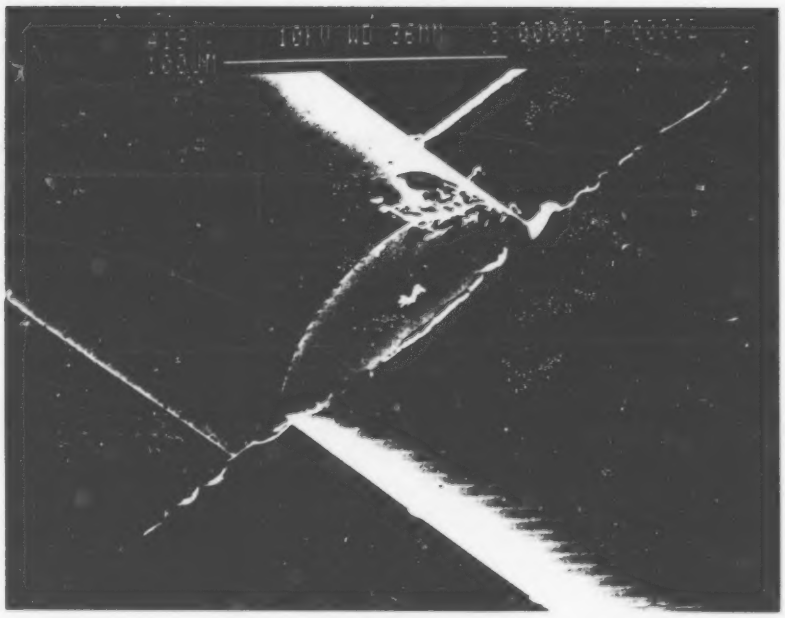

(b)

Fig 4.14 Photographs of single fiber assembled in alignment groove

touches the groove it bends and conforms to the v-groove. The fiber is adjusted until it butts against the waveguide. The detector is placed on a micropositioner with the sensitive surface facing down and is brought down very close to the end facet of the waveguide. The reading on the lock-in amplifier is maximized by adjusting the micropositioner. The detector is brought down until it just touches the silicon surface (reading P_2). The loss is given by $10 \log_{10} P_2/P_1$.

From our measurements, the loss was 4.79 +/- 0.25 dB. Assuming a loss of 1 dB due to the waveguide (1 dB/cm x 0.55 mm = 0.55 dB loss) and the end facet coupling (90% reflectivity of end facet gives 0.45 dB loss), the coupling loss of the fiber in the alignment groove is about 3.8 dB. This coupling loss can be further reduced by using an index matching fluid between the fiber and the waveguide. The precision in alignment is confirmed from Fig. 4.14 (b) where calculations show that the core of the fiber just lies below the surface of the polymer.

CHAPTER 5

CONCLUSION

5.1 Summary of Work

We have developed low loss polymer waveguides in silicon v-grooves by a simple process. Waveguides in v-grooves are compatible with alignment v-grooves. The losses in the waveguide are difficult to determine because of their dependence on surface roughness, but are typically on the order of 1 dB/cm. Taps which couple light out-of-plane have been integrated in the v-grooves. Of the two types of taps investigated, the inside taps are advantageous in terms of their mode insensitivity, space occupied and concentration of tapped beam. The inside taps are designable with a knowledge of the etch rates of the various planes involved. A 12 x 12 tapping array has been designed, fabricated and tested. The tapping array is compatible with standard fiber ribbon cable. Although the testing did not produce uniform tapped power results, it may be possible to achieve this by better design and controlled etching. The 12 x 12 tapping array is suitable as a light distribution system in a hybrid integrated optoelectronic switching matrix. Coupling from a fiber to the waveguide using alignment grooves has also been demonstrated. The coupling loss is estimated to be around 3.8 dB without index matching fluid between the fiber and the waveguide.

5.2 Feasibility in Commercial Applications

An application of the polymer waveguides which has been demonstrated recently is in a optical ribbon connector [35]. In this device, signals from a fiber ribbon cable are deflected onto an array of twelve detectors using the end facets as mirrors. The coupling of the fibers to the waveguides was achieved by using alignment grooves. Applications of the waveguide with taps are in signal processing, signal distribution and switching technology. When compared with other technologies for fabricating optical signal distribution media such as GaAs and $LiNbO_3$, silicon processing is less expensive for the same performance. A competing technology for polymer waveguides is high silica. The advantage of using sidewall taps in silicon v-grooves is the ease of fabrication of out-of-plane tapping structures and the flat surface available at the top of the wafer which makes it suitable for flip-chip mounting. The hybrid nature of the waveguides with taps also makes it useful as a multichip substrate.

The fabrication of the tapping array can be made to have high yield by automating the doctorblading and polishing process. The dispensing of the adhesive can also be automated by using a syringe which dispenses precise amounts of adhesive by computer control into the waveguide trenches without generating any excess. The polishing process would then be unnecessary and the losses could be measured more accurately.

5.3 Suggestions for Future Work

To accurately budget power in any optoelectronic system, it is necessary to know the losses of the individual components. It would be useful to determine the losses in the polymer waveguide accurately. After determining the loss, it is necessary to establish the consistency of these losses. Losses at other wavelengths are also needed. It is also worthwhile to subject the waveguide to temperature cycles and measure the losses. We have demonstrated the application of a cladding layer, but more work is required to reduce the cladding layer thickness and measure the corresponding loss. This could be

done by heating the adhesive to reduce its viscosity prior to spinning it on. Active devices like lasers might be fabricated in these waveguides if the core of the waveguide is doped with a laser dye.

In the fabrication of taps, it would be convenient to have a consistent and homogeneous etch solution. The samples could then be removed at the predetermined time instead of requiring inspection at regular intervals. Techniques of etching taps without generating undesirable interface planes should also be investigated. Finally, more experiments are required to reduce the coupling loss from a fiber to the waveguide.

BIBLIOGRAPHY

1. D. H. Hartman, "Digital high speed interconnects: a study of the optical alternative," *Optical Engineering*, vol. 25, no. 10, pp. 1066-1102, 1986.

2. L. D. Hutchenson and P. Haugen, "Optical interconnects replace hardwire," *IEEE Spectrum*, pp. 30-35, March 1987.

3. P. R. Haugen, S. Rychnovsky and A. Husain, "Optical interconnects for high speed computing," *Optical Engineering*, vol. 25, no. 10, pp. 1076-1085, 1986.

4. J. W. Goodman, F. J. Leonberger, S. Kung and R. A. Athale, "Optical interconnects for VLSI systems," *Proc. IEEE*, vol. 72, no. 7, pp. 850-865, 1984.

5. H. Nishihara, M. Haruna and T. Suhara, *Optical Integrated Circuits*, p. 159, McGraw-Hill Optical and Electro-optical Engineering Series, 1987.

6. L. D. Hutcheson, "Integrated Optics," *Optics News*, p. 8, February 1988.

7. C. H. Henry, G. E. Blonder and R. F. Kazarinov, "Glass waveguides on silicon for hybrid optical packaging," *J. Lightwave Technol.*, vol. 7, no. 10, pp. 1530-1539, 1989.

8. D. G. Hall, "The role of silicon in integrated optics," *Optics News*, pp. 12-15, February, 1988.

9. J. T. Boyd, R. W. Wu, D. E. Zelmon, A. Naumaan, H. A. Timlin and H. E. Jackson, "Guided wave optical structures utilizing silicon," *Optical Engg.*, vol. 24, pp. 230-234, 1985.

10. F. S. Hickernell, "Optical waveguides on silicon," *Solid State Tech,*. p. 83, 1988.

11. J. S. Harper and P. F. Heidrich, "High density multichannel optical waveguides with integrated couplers," *Wave Electronics*, vol. 2, p. 369, 1976.

12. W. T. Tsang, C. C. Tseng, and S. Wang, "Optical waveguides fabricated by preferential etching," *Appl. Optics*, vol. 14, p. 1200, 1975.

13. Y. Kokobun, T. Baba and K. Iga, "Silicon optical printed circuit board for three-dimensional integrated optics," *Electron. Lett*, vol. 21, p. 508, 1985.

14. S. L. Chen and J. T. Boyd, "Integrated optical beam splitters formed in glass channel waveguides having variable weighting as determined by mask dimensions," *IEEE J. Quant. Electron.*, vol. QE-18, p. 1072 , 1982.

15. J. T. Boyd and S. Sriram, "Optical coupling from fibers to channel waveguides formed on silicon," *Appl. Optics*, vol. 17, no. 6, p. 895-898, 1978.

16. M. Veilleux, "A broadband 10x10 optoelectronic switch matrix," M. Sc Thesis, University of Alberta, 1990.

17. R. I. MacDonald, "Optoelectronic matrix switching," *Can. J. Phys.*, vol. 67, p. 390, 1989.

18. R. I. MacDonald, D. K. W. Lam and B. A. Syrett, "Hybrid optoelectronic integrated circuit," *Appl. Optics*, vol. 26, no. 5, p. 842, 1987.

19. J. M. Hagerhorst-Trewhalla, J. D. Gelorma and B. Fan, "Polymeric optical waveguides," *SPIE Integrated Optics and Optoelectronics*, vol. 1177, p. 379, 1989.

20. G. Fitzpatrick, AMC, private communication.

21. H. P. Weber, W. J. Tomlinson and L. A. Chandross, "Organic materials for integrated optics," *Optical and Quantum Electronics*, vol. 7, p. 466, 1975.

22. S. J. Lalama, J. E. Sohn and K. D. Singer, "Organic materials for integrated optics," *SPIE Integrated Optical Circuit Engineering II*, p. 168, 1985.

23. L. M. Walpita, "Organic materials in future integrated optoelectronic circuits," *SPIE Integrated Optics and Optoelectronics*, p. 58, 1989.

24. R. R. Krchnavek, G. R. Lalk and D. H. Hartman, "Laser direct writing of channel waveguides using spin-on polymers," *J. Appl. Phys.*, vol. 66, no. 11, pp. 5156-5160, 1989.

25. D. H. Hartman, G. L. Lalk, J. W. Howse and R. R. Krchnavek, " Radiant cured polymer optical waveguides on printed circuit boards for photonic interconnection use," *Appl. Optics*, vol. 28, no. 1, pp. 40-47, 1989.

26. D. H. Navon, *Electronic Materials and Devices*, pp. 28-36, Houghton Mifflin Company, 1975

27. A. Reisman, M. Berkenblit, S. A. Chan, F. B. Kaufman and D. C. Green, "The controlled etching of silicon in catalyzed ethylenediamine-pyrocatechol-water solutions," *J. Electrochem. Soc.*, vol. 126, no. 8, p. 1409, 1979.

28. M. M. Schlacter, E. S. Schlegel, R. S. Keen Jr., R. A. Lathaen and G. L. Schnable, "Advantages of vapor-plated phosphosilicate films in large-scale integrated circuit arrays," *IEEE Trans. on Electron Devices*, p. 1079, December 1970.

29. P. K. Tien, "Light waves in thin films and integrated optics," *Appl. Optics*, vol. 10, no. 11, pp. 2395-2413, 1971.

30. N. Nourshargh, E. M. Starr, N. I. Fox and S. G. Jones, "Simple Technique for measuring attenuation of integrated optical waveguides," *Electron. Lett.*, vol. 21, p. 818, 1985.

31. Y. Okamura, S. Yoshinaka and S. Yamamoto, "Measuring mode propagation losses of integrated optical waveguides: a simple method," *Appl. Optics*, vol. 22, no. 23, p. 3892, 1983.

32. W-T. Tsang and S. Wang, "Thin-film beam splitter and reflector for optical guided waves," *Appl. Phys. Lett*, vol. 27, no. 11, p. 588, 1975.

33. S. Kumar, R. I. MacDonald and J. N. McMullin, "Low-loss multimode polymer waveguides with serial out-of-plane taps," Optical Fiber Communication Conference, FA8, San Jose, Calif., February 2-7, 1992.

34. M. M. Abu-Zeid, "Corner undercutting in anisotropically etched isolation contours," *J. Electrochem. Soc., Solid-State Science and Technology*, vol. 131, no. 9, pp. 2138-2142, 1984.

35. S. B. Kumar, "Connectors for fiber ribbon cables," Report made for Digital Equipment of Canada Ltd., Kanata, Ontario, May, 1992

36. Norland Products technical data, Norland Products Inc., New Jersey.

37. S. M. Sze, *Physics of Semiconductor Devices*, 2nd edition, John Wiley & Sons, 1985.

38. E. D. Palik, *Handbook of Optical Constants of Solids*, Academic Press, Orlando, p. 760, 565, 1985.

APPENDIX A SUMMARY OF EVALUATION OF OPTICAL MATERIALS

Trade name	Chemical name	Mixing ratio	Curing schedule	Remarks
1. Epotek 301	Epoxy	Part A:4, Part B:1	Air dry overnight followed by 65C for 1 hour	Shrinks on curing.
2. Epotek 302	Epoxy	Part A:1, Part B:1		Soft and shrinks on curing.
3. Epotek 310	Epoxy	Part A:2, Part B:1		Soft and shrinks on curing.
4. Esterex 103	Polyester resin	Part A:10, Part B:1	Air dry for 2 hours	Shrinks on curing and peels off easily from v-grooves during polishing.
5.Dymax Multicure 984	Acrylic	Single component	5mJ/cm2 for 30s followed by 100C for 30 min	Peels off gradually during polishing.Turns amber if excess curing is done.
6.Crystal bond	Propr.*	Single component	Softens at ~60C. Bubbles start leaving at ~135C.Starts shrinking and smoking after prolonged heating.	Cannot be subjected to high temperatures.
7. 9653-1	Polyurethane	Part A:1, Part B:1	30 min air drying, 65C for 1 hour	Two component material.
8. Lytron 5202	Polystyrene	Single component	100C for 15 min	Flakes during curing.
9. CP-82	Acrylic	Pellets:10gm,Methylene Chloride:10 ml	Air dry for few hours, 70C for 1 hour	Film is soft and bubbles up because of trapped solvents .
10. S-28-1	Silicone	Single component	Air dry overnight, 50C for 1 hour	Film cracks during heat curing.
11. S-30	Silicone	Single component	Air dry overnight, 50C for 1 hour	Film cracks during heat curing.
12. Silica film 10,000	Silica in solvent	Single component	Spread - 200 rpm for 7s Spin - 3000 rpm for 15s Acceleration: 700 200C for 15 min, 500C for 1 hour	15 to 20 µms thick films achieved. Manual coating without high temp gives delicate thick film.
13. Silica film undoped	Silica in solvent	Single component	Same spin recipe as silica 10,000 215C for 30 min	Small amounts of silica occur at bottom of groove. Manual coating causes cracking.
14. Silica film boron doped	Silica in solvent	Single component	Same spin recipe as silica 10,000 215C for 30 min	Same as undoped silica film.
15. Dental cement	Acrylic	Monomer:10ml Polymer:10gm	Stir monomer and polymer and cure at 70C for 1 hour	Material is translucent with innumerous bubbles.

All materials had bubbles which were removed partially by keeping in vacuum jar.
*-Proprietary

APPENDIX B PROPERTIES OF MATERIALS [36, 37, 38]

Norland Optical Adhesive 61

NOA 61 is single component clear, colourless, liquid photopolymer that will cure when exposed to ultraviolet light. It has excellent adhesion to metals, fiber glass and glass filled plastics. It also exhibits low shrinkage and stress relieving characteristics. Curing wavelength is 354 to 378 nm. The curing time depends on the thickness of the sample. Some of the typical properties of NOA 61 are:

Viscosity	350 cps
Refractive index	1.56 at λ = 587 nm
Modulus (psi)	150, 000
Tensile (psi)	3, 000
Shore D hardness	85
Transmission	97 % at 630 nm, 1mil thick sample, normal incidence

When finally cured NOA 61 has very good adhesion and solvent resistance, but it has not reached its optimum adhesion. This will come with aging over a period of about 3 weeks in which a chemical bond will form between the glass and adhesive. This optimum adhesion will also occur in 12 hours at 50° C. Doublets bonded with NOA can withstand thermal shocks before aging from -15°C to 60°C. After aging, they will withstand temperature conditions from -80°C to 90°C. Shelf life of the liquid is at least 4 months if kept in the original container.

Norland Optical Adhesive 81

NOA 81 is a single component liquid adhesive that cures in seconds to a tough, hard polymer when exposed to UV light. Curing time depends on sample thickness. It has good adhesion to glass, metals, PCB and other glass filled plastics. This adhesion improves with age with optimum adhesion reached after aging for 1 to 2 days. The cured adhesive can withstand temperatures from -150°C to 125°C. Shelf life of the liquid is at least 4 months if kept in the original container.

Some typical properties are:

Solids	100%
Viscosity	300-300 cps
Refractive index	1.56 at λ = 587 nm
Elongation at failure	25%
Modulus (psi)	200, 000
Tensile (psi)	4, 000
Shore D hardness	90
Transmission	97 % at 630 nm, 1mil thick sample, normal incidence

Norland Optical Adhesive 68

NOA 68 is a single component optically clear adhesive that cures with UV light. It has good adhesion to many plastics such as acrylic, polycarbonate and CAB. In addition, NOA 68 has good adhesion to glass and metals and because it is flexible, it can be used to

bond combinations of the three. Shelf life of the liquid is 4 months at room temperature. Some of is properties are:

Viscosity	5, 000 cps
Modulus (psi)	20, 000
Tensile (psi)	2, 500
Elongation at failure	80%
Shore D hardness	60
Refractive index	1.54 at λ = 587 nm

Silicon (Si)

Crystal structure	Diamond
Thermal conductivity	1.5 W/cm-^{o}C at 300K
Energy gap	1.12 eV at 300 K
Density	2.328 g/cm^3
Refractive index	3.882 - j0.019 at 632.6 nm

Silicon dioxide (SiO_2)

Structure	Amorphous
Melting point	~ 1600 ^{o}C
Density	2.2 g/cm^3
Energy gap	9 eV
Refractive index	1.456 at 643.85 nm

APPENDIX C POSITIVE PHOTORESIST PHOTOLITHOGRAPHY RECIPE

a) Thermal oxidation

First, a layer of silicon dioxide (~0.5 μm) is grown on the wafer by thermal oxidation in a quartz furnace. The oxidation is carried out in a nitrogen-water vapour atmosphere (flow rate is 0.75 l/min at 20 psi) at a temperature of 1050 °C.

b) Photoresist spin-on

This is done by placing the wafer on the vacuum chuck of the spinner and programming it with the following parameters:

Acceleration : 700 (corresponds to 465 rpm/s^2)
Spread cycle : 400 rpm for 3 seconds
Spin cycle : 3500 rpm for 15 seconds.

Three cc. of the HPR 504 is taken in a syringe and spread on the wafer prior to spreading.

c) Softbake

The solvent in the resist is removed by softbaking in a preheated oven. The recipe is

Vacuum bake : 10 seconds
Nitrogen back fill : 50 seconds
Temperature of hot plate : 110°C

d) Exposure

The photoresist is exposed for 11 seconds under a 200 W mercury lamp.

e) Developing

The exposed wafer is taken and placed on the vacuum chuck of the spinner. The process parameters used are:

Pre-wet (deionised water) : 400 rpm for 5 seconds
Develop : 400 rpm for 50 seconds
Rinse : 400 rpm for 90 seconds
Spin dry : 3500 rpm for 15 seconds

f) Hardbake

The developed sample is hardbaked in a preheated oven to improve the adhesion of the resist to the oxide. The oven parameters are:

Nitrogen backfill : 10 seconds
Vacuum bake : 50 seconds
Temperature of hot plate: 120°C

APPENDIX D MASKS USED FOR DEVELOPING WAVEGUIDES AND TAPS

Mask 1 (See Fig. D-1)

This was the first mask designed to investigate the feasibility of using silicon v-grooves as waveguides. The mask contained patterns for straight waveguides (locations A, B), waveguides with curves (locations C and D), splitters (location E) and crossed waveguides (location F). The straight line patterns yielded grooves with smooth sidewalls and could be used to make low loss waveguides. The curved lines yielded rough surfaces because of the correction planes formed due to misalignment with the <110> direction and were not usable. The waveguide splitters also yielded rough sidewalls for the same reason. The crossed patterns were originally designed to test the possibility of intersecting waveguides. However, due to the undercutting at 90^{o} corners, bevelled planes appeared at the corners and it first gave us the idea of out-of-plane outside taps. For placing optical fibers against the waveguides, a larger etch window width was provided at the end of the waveguide etch window (location G). Due to the undercutting, the junction of the smaller and larger v-groove was smoothened and could not be used for placing fibers tightly against the waveguides.

Mask 2 (See Fig. D-2)

In the second mask, patterns were designed for waveguides (location H), waveguides with inside taps (location I), waveguides with outside taps (locations J and K) and splitters (location L). The waveguides were longer (~ 7cm) since loss measurements could not be made accurately with the shorter waveguides from mask 1. The outside taps were designed with different sizes of openings to control the tapping ratios. The inside taps were provided with the same size of rectangles in each waveguide to study the etching shapes. The splitters which had curved branches instead of straight branchs

yielded rough sidewalls as before. There were patterns for generating centre taps for use by other researchers.

Mask 3 (See Fig. D-3)

This mask had patterns for single mode waveguides, multimode waveguides of varying lengths and multimode waveguides with centre taps for other researchers. The mask also had patterns for 12 x 12 tapping arrays (locations M and N) which we used.

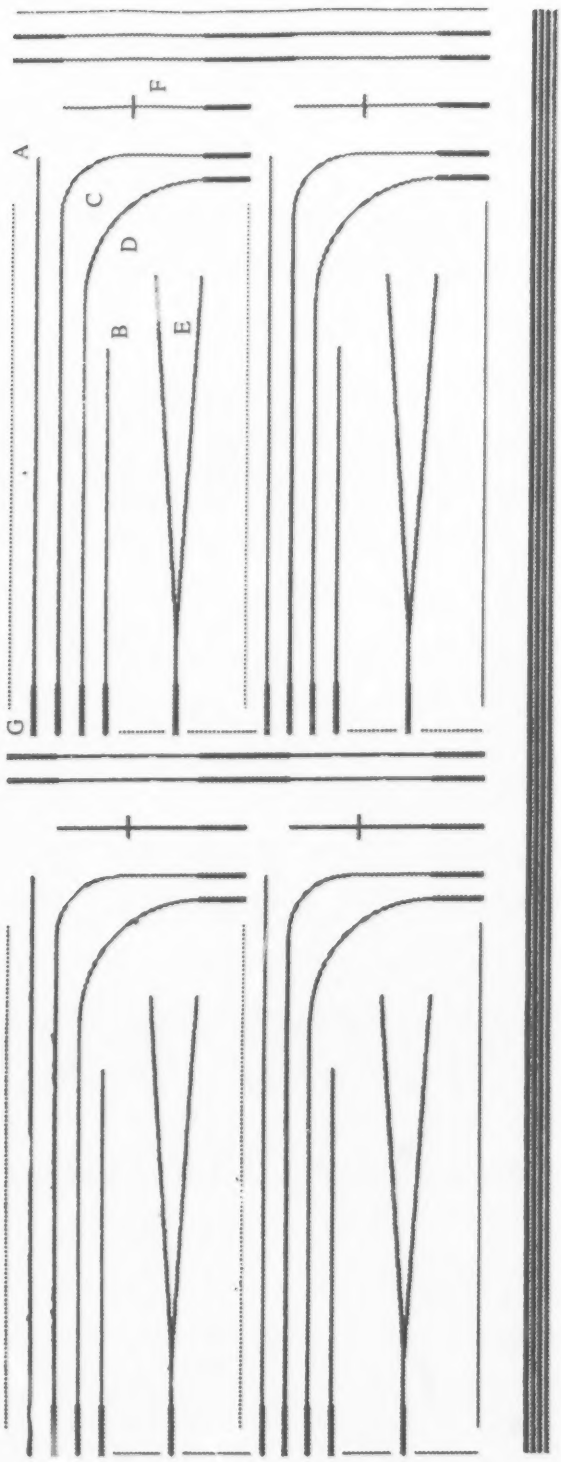

Fig. D-1 Mask 1

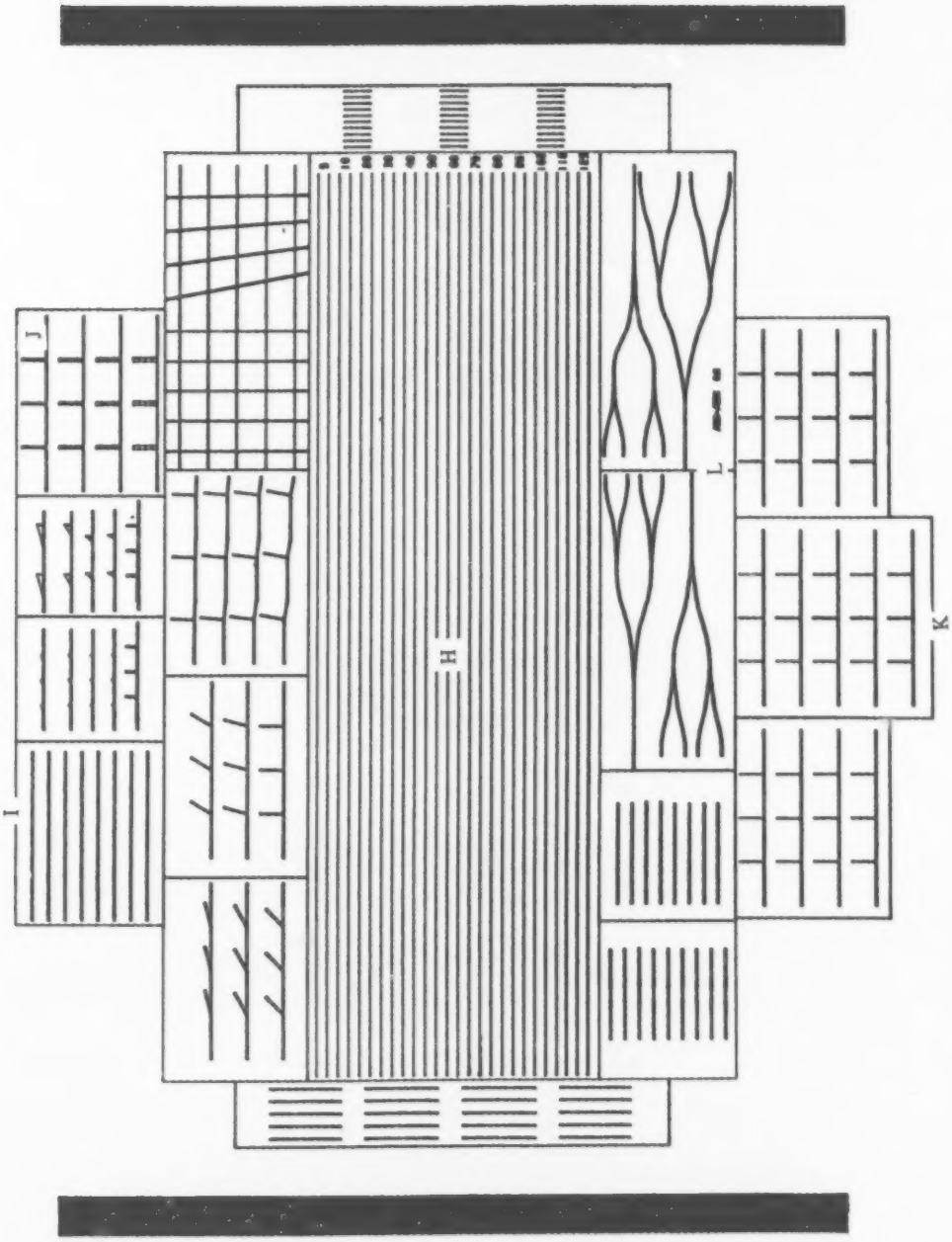

Fig. D-2 Mask 2

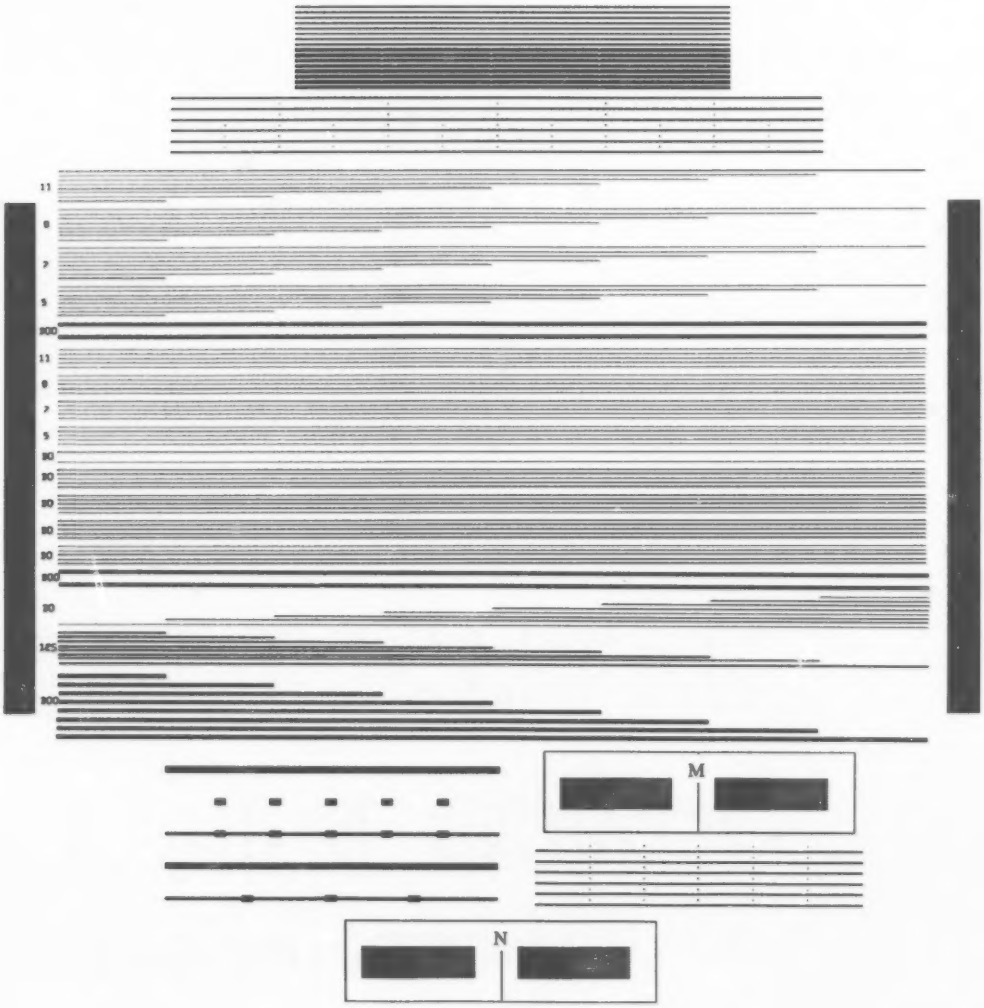

Fig. D-3 Mask 3

APPENDIX E METALLIZATION OF TAPS

(Please refer to Fig. E-1)

The wafer with CVD oxide was coated with Al in a thermal evaporator. This is done by placing a wire of pure Al on a tungsten boat in a vacuum chamber (pressure ~10^{-6} Torr) and heating up the boat by passing current (100 to 150 A). The Al first melts, evaporates and then is deposited on the wafers mounted on a target plate above the boat. The thickness of the Al film was monitored with a crystal thickness monitor. We deposited 0.1 μm of Al which gave a reflectivity of ~90% at 630 nm (air-Al-oxide-Si, normal incidence). The reflectivity degrades by a few percent with time due to the formation of Al_2O_3.

Negative photoresist (HNR 80) is spun on the wafer in a spinner. The spinner is programmed with the following parameters:

Spread: 400 rpm for 4 seconds

Spin speed: 6000 rpm for 15 seconds

Acceleration: 100 (corresponds to 2250 rpm/s^2)

Lower acceleration (>100) results in a wrinkled photoresist film. Negative resist is dispensed from a beaker prior to the spread cycle. A resist thickness of 0.5 μm was obtained.

The wafer is softbaked to dry the resist film in a preheated oven. The oven parameters are:

Vacuum bake: 2 seconds

N_2 backfill: 8 minutes

Temperature of plate: 85°C

Selective exposure of the photoresist was obtained without a mask. The spot from the objective of a microscope was used to define the exposed region and the exposure was obtained by removing a UV filter in the light path. The additional advantage of this

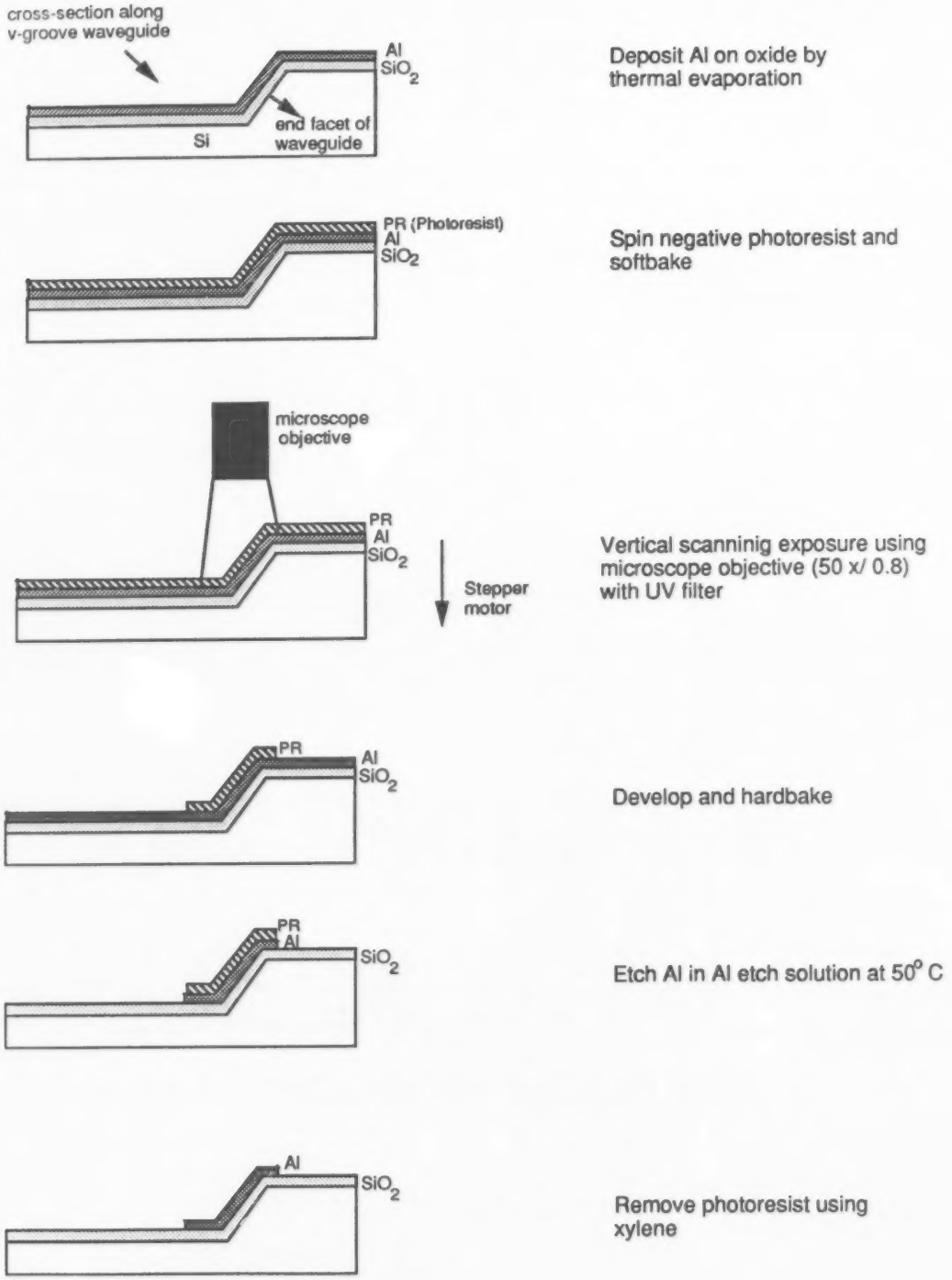

Fig.E-1 Negative photoresist method of patterning Al on oxide
(diagram not to scale)

method is that the area to be exposed can be clearly viewed using the eyepiece of the microscope. Larger magnifications and higher numerical apertures of the objective lens gave smaller spots. We chose a 50X objective (0.8 N.A) which gave medium sized spots. The spot size could be adjusted to ~150 μm by adjusting a variable field diaphragm in the path of the light. The depth of focus obtained was ~0.4μm. In v-grooves which are ~90 μm deep, it was necessary to scan the area to be exposed vertically with the objective lens so that the resist polymerizes all along the sloped coupling planes. This can be achieved by focusing at the bottom of the v-groove and lowering the stage holding the sample in steps of 0.05 μm by means of a stepper motor. This scan takes about 100 seconds and was repeated three times to get better exposure of the resist on the slopes. After developing, a spot of resist remains on the Al [step 4 of Fig. E-1]. The developers used were xylene and butyl acetate. The wafer is placed on the vacuum chuck of the spinner. The developing recipe is:

Xylene dispense: 1000 rpm for 20 seconds

Overlap: 2000 rpm for 2 sec

Butyl acetate rinse: 1000 rpm for 8 seconds

Spin dry: 4000 rpm for 8 seconds

The wafer was next hardbaked in an oven to improve the adhesion of the photoresist. The oven parameters are:

Vacuum bake: 2 seconds

N_2 backfill: 8 minutes

Temperature of plate: 140°C

The resulting wafer with the patterned resist was etched in an Al etch (phosphoric acid) solution at 50°C in a water bath heater. The sample was agitated by stirring the solution with the sample so that uniform etching of Al takes place. The resist was next removed by washing the wafer in xylene. The wafer was inspected under a microscope to verify that the spots have been patterned properly.

APPENDIX F ALIGNMENT OF FIBER PROBE TO WAVEGUIDE

A visual technique for aligning the fiber probe to the waveguide is described here. The misalignment in the setup introduces artificial losses or even gain to the actual losses in the waveguide. The important errors that can occur as the fiber probe travels along the waveguide are:

a) Angular travel

Errors will occur if the fiber probe travels at an angle with respect to the waveguide. This error can be eliminated by adjusting the fiber probe for maximum power across the waveguide at each point of the measurement.

b) Height variation

Errors will occur if the distance between the fiber probe end and the waveguide surface increase or decrease as the fiber probe travels along the waveguide.

Before the silicon piece is fixed to the platform, the platform is adjusted to be approximately at level using a bubble level indicator. The silicon piece is fixed to the platform so that the centre of the waveguide coincides with the perpendicular line (OT) from the translation stage to the centre of rotation (COR) of the horizontal rotation stage (See Fig. F-1). A glass fiber is next placed on the micropositioner instead of the fiber probe. A hole had been drilled through the fiber holder so that the fiber end can be viewed with a microscope. The angular travel alignment is done first as explained below.

1) Travel alignment

Move the alignment fiber until it gently touches the waveguide at x cm from the line OT (See Fig. F-1). Using the screw gauge on the micropositioner, move x cm to the one side of the OT (point A). Using the horizontal rotation stage rotate the platform so that the fiber is now at the midpoint (point C) between the waveguide (point B) and the previous position (point A). Now, the angular misalignment is reduced. Perform the same procedure a couple of times so that near-perfect angular alignment is achieved. While making the fiber travel along the waveguide, it is a recommended that the fiber be raised vertically about 100 μm so that it does not scratch the waveguide.

2) Height alignment

In this procedure, the fiber is made to touch the waveguide softly at a distance x cm from the line (OT) where OT is the perpendicular line from the translation stage to the COR of the second rotation stage (See Fig. F-2). The reading on the vertical screwguage of the micropositioner holding the fiber is noted. Let it be h1. The fiber is withdrawn 500 μm from the surface and then made to touch the waveguide at a distance x cm on the other side of the line OT (E). The reading is taken on the vertical screw gauge. Let it be h2. Next withdraw the fiber from the waveguide surface to a distance of mod(h1-h2)/2. Adjust the vertical rotation stage so that the waveguide surface just contacts the fiber end. Now, the height misalignment has been reduced. Repeat this procedure until near-perfect height alignment is achieved.

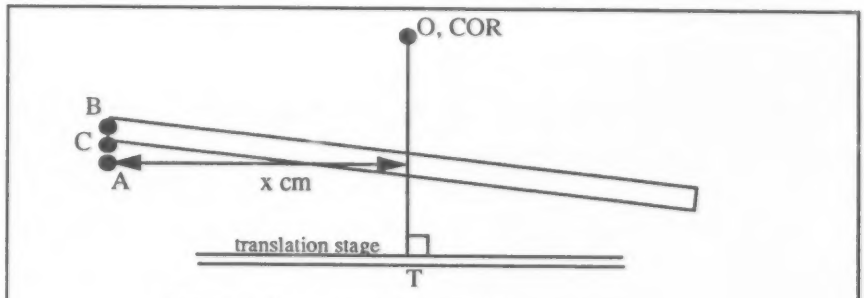

Fig. F-1 Top view of waveguide

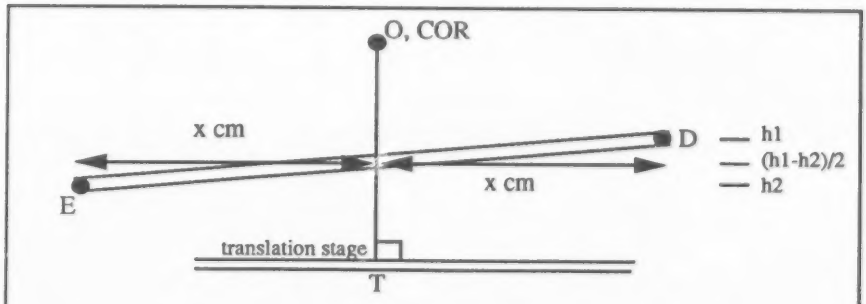

Fig. F-2 Sideview of silicon sample

APPENDIX G DERIVATION OF TAPPING SIZE D_n

(Please refer to Fig. 4.8)

Let the fraction of power tapped $r_n = A_n/A_{tot}$. Let P_o be the power available at the input of the waveguide and $T_1, T_2, ...T_N$ be the power tapped at tap 1, 2, ...N where N is the total number of taps in the waveguide. Then,

$T_1 = (A_1/A_{tot}) P_o$.

$T_2 = (A_2/A_{tot})(P_o-T_1)$.

$T_3 = (A_3/A_{tot})(P_o-T_1-T_2)$ and so on.

Generally,

$T_n = (A_n/A_{tot})[P_o-(T_1+T_2+ ....T_n)]$.

$T_1=T_2=T_3= .....T_N = T$ for equal tapped power from all taps.

Now, $T_n = r_n[P_o-(n-1)T] = T$.

Hence $r_n = T/[P_o-(n-1)T] = 1/[P_o/T - (n-1)] = 1/[N-(n-1)]$.

Now, $A_{tot} = (1/2.W)(W/\sqrt{2}) = W^2/(2\sqrt{2})$ (because width of groove = $\sqrt{2}$ depth of groove.)

and $A_n = A_{tot} - (W-D_n)^2/(2\sqrt{2})$.

Therefore, $r_n = A_n/A_{tot} = 1 - (W-D_n)^2/W^2 = 1/[N-(n-1)]$ from above.

Solving for D_n,

$D_n = W[1- \sqrt{(N-n)/(N-n+1)}]$.

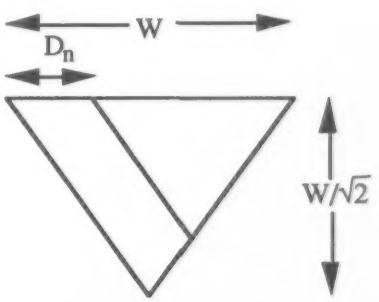

Fig. 4.8

APPENDIX H DETERMINATION OF ETCH RATE OF (212)-(212) CORNER

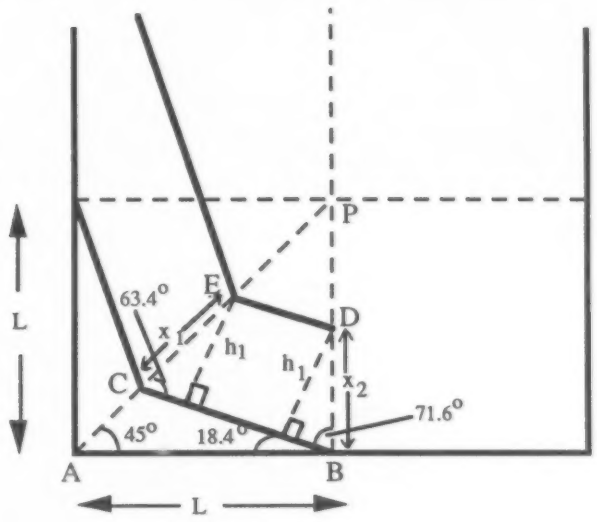

We have to calculate the etch rate in direction AP. We already know t_m (which is the etch time for the undercut to reach E and D), length L and distance DB.

The etch rate in direction AP = AE/t_m.

For a given AB, AC is always constant.

The AP etch rate = $AE/t_m = (AC + CE)/t_m$.

From the geometry illustrated in the diagram, AC = 0.353L and CE = 1.061DB.

Therefore, the AP etch rate = $(0.353L + 1.061DB)/t_m$.

APPENDIX I DESIGN OF TAPPING ARRAY WITH ALIGNMENT GROOVES

(A) Alignment grooves

The alignment groove is designed such that the core of the fiber in the groove matches with the waveguide core.

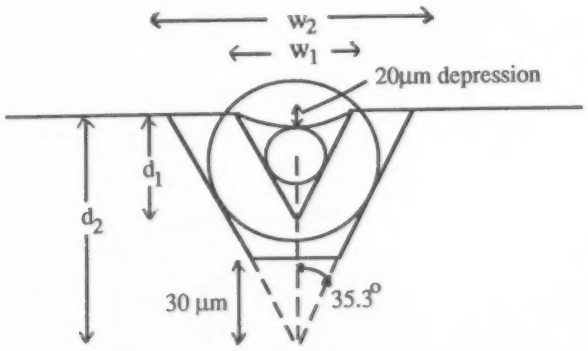

The depth of the alignment groove $d_2 = 20 + 25 + 62.5/\sin(35.3) \sim 153$ μm.
The depth to be etched is 153 - 30 = 123 μm since the alignment groove does not have to etched all the way to support the fiber. For the given etch depth, and using an etch rate of 0.64 μm/min, the required etch time is 192 min..
In 192 min, the over-etch of the alignment grooves ~ 11 μm (assuming <111> etch rate is ~0.03 μm/min)

The width of the alignment groove $w_2 = \sqrt{2}d_2 \sim 217$ μm (The designed width on the mask was 206 μm to compensate for the <111> over-etching.)
Now, depth of the waveguide groove $d_1 = 20 + 25 + 25/\sin(35.3) \sim 88$ μm
Therefore, $w_1 = \sqrt{2}d_1 \sim 125$ μm

With <111> over etch, the final width of waveguide is 125 + 11 = 136 μm and the corresponding v-groove depth is 96.5 μm.

(B) Tapping array mask

The tap sizes (D_n) for W = 136 μm and N = 12 are got by using equation 4 of Chapter 4.

$D_1 = 5.81$ μm, $D_2 = 6.35$ μm, $D_3 = 7.01$ μm, $D_4 = 7.81$ μm, $D_5 = 8.82$ μm, $D_6 = 10.13$ μm, $D_7 = 11.90$ μm, $D_8 = 14.41$ μm, $D_9 = 18.29$ μm, $D_{10} = 25.05$ μm, $D_{11} = 39.99$ μm, $D_{12} = 136.53$ μm

The size of the compensation square is calculated as follows (See figure below):

AP = 0.353 x 192.19 = 67.84 μm

Adding a tolerance of 10% in the size to account for varying etch rate gives 74.62 μm

PB = sin(45) x 74.62 ~ 53 μm

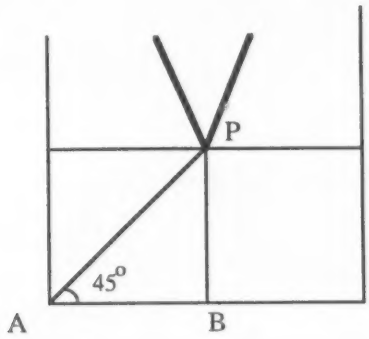

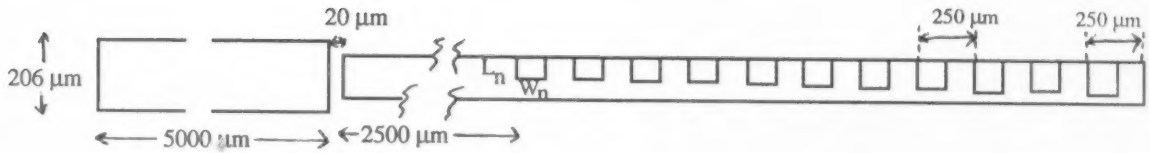

L_n and W_n are the length and width of the mask for tap n.

W_n = 2 x 53 = 106 μm which is the same for all the tap masks.

L_1 ~ 59 μm, L_2 ~ 59 μm, L_3 ~ 60 μm, L_4 ~ 61 μm, L_5 ~ 62 μm, L_6 ~ 63 μm, L_7 ~ 65 μm, L_8 ~ 67 μm, L_9 ~ 71 μm, L_{10} ~ 78 μm, L_{11} ~ 93 μm.

The spacing between the alignment groove etch window and the waveguide etch window is 20 μm.